

Supporting Information for

Ferrocene-derived Fe-metalated porous organic polymer for the core planarity-triggered detoxification of chemical warfare agents

Ratul Paul,^{[a,b],§} Chitra Sarkar,^{[a,b],§} Manjari Jain,^{[c],§} Shaojun Xu,^[d,e] Kashmiri Borah,^[f] Duy Quang Dao,^[g] Chih-Wen Pao,^[h] Saswata Bhattacharya*,^[c] & John Mondal*,^[a,b]

[a] R. Paul, C. Sarkar and Dr. J. Mondal

Catalysis & Fine Chemicals Division, CSIR-Indian Institute of Chemical Technology, Uppal Road, Hyderabad 500 007, India. Email: johnmondal@iict.res.in, johncuchem@gmail.com (J.M.)

[b] R. Paul, C. Sarkar and Dr. J. Mondal

Academy of Scientific and Innovative Research (AcSIR), Ghaziabad- 201002, India.

[c] M. Jain and Dr. S. Bhattacharya

Department of Physics, Indian Institute of Technology Delhi, Hauz Khas, New Delhi 110 016, India. Email: saswata@physics.iitd.ac.in (S.B.)

[d] Dr. S. Xu

Cardiff Catalysis Institute, School of Chemistry, Cardiff University, Cardiff CF10 3AT, U.K.

[e] Dr. S. Xu

UK Catalysis Hub, Research Complex at Harwell, Rutherford Appleton Laboratory, Harwell, OX11 0FA, United Kingdom.

[f] K. Borah

Polymers & Functional Materials Division, CSIR-Indian Institute of Chemical Technology, Uppal Road, Hyderabad 500 007, India.

[g] Dr. D. Q. Dao

Institute of research and development, Duy Tan University, Da Nang, 550000, Viet Nam.

[h] Dr. C. W. Pao

National Synchrotron Radiation Research Center, 101 Hsin-Ann Road, Hsinchu 30076, Taiwan.

§R.P., C.S. and M.J. equally contributed in this work.

Table of content

Sl. No.	Context	Page No.
1	Characterization Details	S3
2	Experimental Section	S4
3	Table S1: Elemental C, H, N analysis	S7
4	Table S2 : Cartesian coordinates and thermochemical properties of two POP structures calculated in the gas phase at the B3LYP/Def2-SV(P) level of theory	S7
5	Thermo Gravimetric Analysis (TGA)	S20
6	Wide angle Powder X-ray Diffraction pattern (PXRD)	S21
7	Optimized geometry of the Fe-Rb-POP and Fe-Tt-POP systems, respectively.	S22
8	N ₂ -adsorption/desorption isotherms	S24
9	Pore Size Distributions of POPs	S25
10	FE-SEM images of POPs	S27
11	TEM images of POPs	S28
12	XPS survey spectra	S29
13	XP-spectra at C-1s core region	S30
14	XP-spectra at N-1s core region	S31
15	Table S3: The table of product distribution under the influence of different reaction conditions such as without catalyst, without H ₂ O ₂ , under N ₂ atmosphere, and at room temperature.	S34
16	Catalytic property tests with Fe-Tt-POP catalyst with various Fe contents under optimized reaction conditions.	S35
17	Time profile for the oxidative decontamination of CEES using Fe-Tt-POP & Fe-Rb-POP catalyst under optimized reaction conditions.	S36
18	Table S4: Previous Reports	S39
19	Table S5: Calculated ΔG values of sulfoxide-O and sulfoxide-S pathway for Fe-Tt-POP and Fe-Rb-POP, respectively.	S40
20	Reusability test	S41
21	Reusable Catalyst Characterization	S42
22	References	S48

Characterization Details:

Powder X-ray Diffraction pattern (PXRD) of different samples were recorded with a Bruker D8 Advance X-ray diffractometer operated at a voltage of 40 kV and a current of 40 mA by using Ni-filtered Cu K α ($\lambda = 0.15406$ nm) radiation. High-resolution Transmission Electron Microscopy (HR-TEM) images were recorded with a JEOL JEM 2010 transmission electron microscope with operating voltage 200 kV, equipped with a Field-emission Electron Gun (FEG). Field-emission scanning electron microscopic images of samples were obtained by using a JEOL JEM 6700 Field-emission Scanning Electron Microscope (FE-SEM). Nitrogen sorption isotherms were obtained by using a Quanta chrome Autosorb 1C surface area analyzer at 77 K. Prior to the measurements, the samples were degassed at 393 K for approximately 4 h under high vacuum. Surface areas were calculated from the adsorption data by using the Brunauer-Emmett-Teller (BET) method in the relative pressure (P/P_0) range 0.01-0.1. The total pore volumes and pore size distribution curves were obtained from the adsorption branches by using Nonlocal Density Functional Theory (NLDFT) method. Fourier Transform Infrared Spectroscopy (FTIR) spectra of the samples were recorded by using a Nicolet MAGNA-FT IR 750 Spectrometer Series II. Solid-state Cross-Polarization Magic Angle Spinning Carbon-13 Nuclear Magnetic Resonance (^{13}C CP MAS NMR) studies were performed by using a Bruker Advance III HD 400 MHz NMR spectrometer. High-angle Annular Dark-field Scanning Transmission Electron Microscopy (HAADF-STEM) and energy-dispersive X-ray mapping images were obtained with a TECNAI G2 F20 equipped with an EDX detector. X-ray Photoelectron Spectroscopy (XPS) was performed with an Omicron nanotech operated at 15 kV and 20 mA with a monochromatic Al K α X-ray source. The Fe K-edge X-ray Absorption Spectra (XAS) were measured using beamline 44A at Taiwan Photon Source (TPS) of the National Synchrotron Radiation Research Centre (NSRRC, Hsinchu, Taiwan). All spectra were performed in transmission mode at room temperature. The incoming and outgoing photon fluxes were measured by ionization chambers filled with appropriate mixtures of N $_2$ and Kr gases. For these measurements, the nanohybrids were uniformly diluted inside an inert boron nitride matrix and pressed to a form of pellet to have absorption edge jump between 0.5 and 1.

All calculations were performed using Gaussian 16 Rev.A.03.^[1] Optimized geometries and frequencies were calculated at the Becke-3 Parameter-Lee-Yang-Parr hybrid functionals B3LYP^[2] combined with the Def2-SV(P) basis set.^[3,4] This basis set was successfully employed by Jorge Gutierrez-Flores *et.al* (2020) to evaluate the stabilization of Tominaga's

M12L24 nanoballs with Pd²⁺ and Ni²⁺ as metal centers.^[5] Frontier molecular orbital distributions including highest occupied molecular orbital (HOMO) and lowest unoccupied molecular orbital (LUMO) and electrostatic potential (ESP) maps are also investigated using Gauss View 6 to predict the electronic properties of the Porous Organic Polymer (POP) units. Density Functional Theory (DFT) calculations were performed using the Vienna *ab initio* Simulation Package (VASP)^[6] with the Projected Augmented Wave (PAW) potential.^[7] The Perdew–Burke–Ernzerhof (PBE)^[8] exchange–correlation functional within the Generalized Gradient Approximation (GGA) was used in all the calculations. The cut-off energy of 500 eV was chosen for the plane-wave basis set. The tolerance energy for the convergence was set to 0.001 meV to achieve self-consistency in the total energy. All the electronic configurations were fully relaxed until the ionic forces were smaller than 0.01 eV/Å using conjugate gradient minimization. Their corresponding binding energies direct towards the type of adsorption in the system.

Experimental Section:

Materials:

All the required chemicals ferrocene carboxaldehyde, pararosanine base, 4,4',4''-(1,3,5-Triazine-2,4,6-triyl) trianiline, benzaldehyde, 2-Chloroethyl ethyl sulfide (CEES), 2-Chloroethyl methyl sulfide (CEMS), dimethyl sulfide (DMS), ethyl methyl sulfide (EMS) and hydrogen peroxide were purchased from Sigma-Aldrich and used as received unless noted otherwise. Dimethyl sulfoxide (DMSO), methanol (MeOH), acetonitrile solvents were all dried before using in reaction.

Synthesis of Pararosanine based ternary Porous-Organic Polymer (Fe-Rb-POP):

In a typical synthetic procedure ferrocene carboxaldehyde (2 mmol, 0.41 gm), Pararosanine Base (4 mmol, 1.22 gm) and Benzaldehyde (2 mmol, 0.102 ml) were mixed with DMSO (12 ml) in a 100 mL two-neck round bottom flask equipped with a stirrer and a condenser. Then, the reaction mixture was stirred under N₂ atmosphere for 1 hour to get a homogeneous mixture. Further, the prepared solution was taken in a seal tube and heated at 140° C for 40 h. Finally, the mixture was cooled down to room-temperature and the product was collected and washed with MeOH for several times and dried in a vacuum oven at 100° C overnight to get the blackish powder.

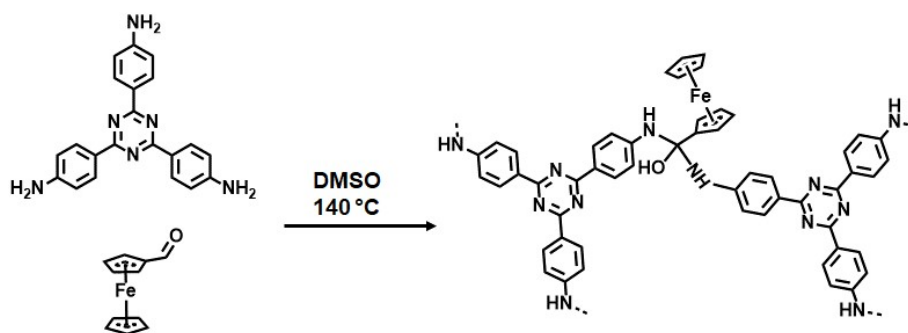
Synthesis of 4,4',4''-(1,3,5-Triazine-2,4,6-triyl) trianiline based ternary Porous-Organic Polymer (Fe-Tt-POP):

Similar synthetic protocol was followed as mentioned above, but instead of Pararosaniline Base, here we use 4,4',4''-(1,3,5-Triazine-2,4,6-triyl) trianiline (2 mmol, 0.708 g).

Among all the conditions screened, the combination of Fe-aldehyde, aromatic amine & aromatic aldehyde (1:2:1) and DMSO as a solvent was the best condition for the synthesis of Fe-metalated POP with high yield (~89%). Both **Fe-Tt-POP** & **Fe-Rb-POP** are black powders, and they are insoluble in water and common organic solvents.

Synthesis of 4,4',4''-(1,3,5-Triazine-2,4,6-triyl) trianiline based binary Porous-Organic Polymer (Fe-Tt-POP-B):

In a typical synthetic procedure ferrocene carboxaldehyde (2 mmol, 0.41 gm) and 4,4',4''-(1,3,5-Triazine-2,4,6-triyl) trianiline (2 mmol, 0.708 g) were mixed with DMSO (12 ml) in a 100 mL two-neck round bottom flask equipped with a stirrer and a condenser. Then, the reaction mixture was stirred under N₂ atmosphere for 1 hour to get a homogeneous mixture. Further, the prepared solution was taken in a seal tube and heated at 140° C for 40 h. Finally, the mixture was cooled down to room-temperature and the product was collected and washed with MeOH and acetone for several times and dried in a vacuum oven at 100° C overnight to get the blackish powder designated as **Fe-Tt-POP-B**.



Scheme S1: Synthetic procedure of **Fe-Tt-POP-B** via binary co-polymerization.

Cyclic Voltammetry (CV) analysis:

Electrochemical studies 5 mg of the **Fe-POPs** were dispersed in a homogenized solvent mixture consisting of 150 μ L ethanol and 30 μ L nafion solution. 10 μ L of this suspension was then drop-casted on a clean glassy carbon electrode as working electrode and dried at RT. Pt foil and Ag/AgCl (3M KCl) were employed as counter and reference electrodes,

respectively. Cyclic voltammetry analysis was performed using OrigaFlex Multichannel system in 0.5 M Na₂SO₄ electrolyte at a scan rate of 50 mV s⁻¹.

Liquid-phase Selective Oxidation of Sulfides to Sulfoxides:

Liquid phase oxidation of sulfides to sulfoxides was performed using Thioanisole (TA) as a model sulfide compound. At first, a well-dispersed mixture of 0.1 ml of TA (0.5 mmol), Fe-POP catalyst (50 mg), and H₂O₂ (0.25 ml) was heated at 100° C for desired time. After the completion of the reaction, the catalyst was separated from the reaction mixture via filtration. Further, the collected reaction mixture was analyzed by a gas chromatograph (Shimadzu 2010) equipped with a flame ionization detector using an INNOWax capillary column (diameter: 0.25 mm, length: 30 m). The products were also identified by GC-MS (Shimadzu, GCMS-QP2010S). After the confirmation of sulfide to sulfoxide conversion, catalytic oxidation of other sulfur mustard (HD) compounds was carried out under similar reaction conditions to convert HDs into less toxic sulfoxide derivatives.

***In situ* Diffuse Reflectance Infrared Fourier Transform Spectroscopy (DRIFTS):**

The *in-situ* DRIFTS experiment was carried out using an Agilent Carey 680 FTIR Spectrometer equipped with a Harrick DRIFTS cell. The spectra were recorded at 4 cm⁻¹ resolution and each spectrum was averaged 64 times. 50 mg of sample was first mixed with 0.12 ml (0.1 mmol) of thioanisole and 0.25 ml H₂O₂ using an incipient wetness impregnation method to form a solid-liquid mixture. Then the incipiently wetted sample was placed into the sample holder in the Harrick DRIFTS cell. Each sample was pre-treated at 30° C using 99.999% argon (Ar, BOC gas Ltd.) at a gas flow rate of 50 ml min⁻¹ for 1h in order to remove the residual air and impurities in the cell. Then the purged sample was taken as the background spectrum. After that the temperature of the sample was rapidly increased to 100° C at a 50° C/min rate under the same Ar gas condition, then maintained at 100° C for 13h to determine the surface intermedia revolution. The sample **Fe-Rb-POP** and **Fe-Tt-POP** was tested using the operando DRIFTS.

Hot-filtration Test:

We have performed hot filtration test for our catalyst to confirm the heterogeneous nature of the **Fe-POPs**. Initial reaction was begun with dispersing 50 mg catalyst, thioanisole (0.5 mmol) in 10ml acetonitrile inside a round bottom flask at 100°C and the reaction was continued for 6 h. After that, the catalyst was removed from resulting solution and the

obtained hot reaction mixture was subjected to GC analysis, which exhibited ~40 and ~16% conversion of thioanisole for **Fe-Tt-POP** and **Fe-Rb-POP**, respectively. Then, the same reaction was carried out at identical condition for 4h utilizing the obtained hot reaction mixture after removing catalyst from the system. There is no obvious increase in conversion above 40 and 16%, confirmed from GC analysis. Absence of metal leaching in the filtered reaction mixture from the catalyst was also confirmed by atomic absorption (AAS) spectroscopy analysis. This analysis clearly indicates successful ternary polymerization between ferrocene aldehyde, benzaldehyde, trainline and para-rosaline unit and the obtained material is indeed heterogeneous in nature. We have also measured Fe contents in the isolated **Fe-Tt-POP** and **Fe-Rb-POP** catalysts by Inductively Coupled Plasma-Mass Spectrometry (ICP-MS) analysis which is about ~1.9 and ~1.96 wt%, respectively. Both of these observations clearly indicate our catalyst is indeed heterogeneous in nature and Fe metal sites are strongly wrapped in such a way so that its leaching has been prohibited.

Table S1: Elemental C, H, N analysis

Catalyst	Nitrogen (wt%)	Carbon (wt%)	Hydrogen (wt%)
Fe-Rb-POP	6.254	72.646	14.249
Fe-Tt-POP	10.947	72.232	12.471

Table S2: Cartesian coordinates and thermochemical properties of two POP structures calculated in the gas phase at the B3LYP/Def2-SV(P) level of theory.

Fe-Tt-POP			
0 1			
C	-2.76974500	8.27339000	4.21654900
N	-3.66221800	7.93935600	3.26058000
C	-4.28857300	6.75555100	3.42692200
C	-3.17005100	6.34406100	5.37875300
N	-2.49565000	7.50977000	5.29574100
N	-4.07023600	5.92225600	4.46598900
C	-5.28281700	6.34892700	2.41052600
C	-5.95848800	5.10890200	2.50255600
C	-5.59129900	7.18759300	1.31770400
C	-6.90150200	4.73067300	1.55032700
H	-5.72088900	4.44384500	3.34685400
C	-6.53609300	6.81852300	0.35722000
H	-5.06443700	8.15066300	1.23476600
C	-7.22521400	5.58045700	0.45751100
H	-7.41584300	3.75839500	1.64272200

H	-6.73969800	7.50990800	-0.47544600
C	-2.91264200	5.47637900	6.54888400
C	-3.56154200	4.22689200	6.69005500
C	-2.01401100	5.87037600	7.56352700
C	-3.32678700	3.41519100	7.79707800
H	-4.25917500	3.90633300	5.90131800
C	-1.77147600	5.06407000	8.67839500
H	-1.49984600	6.83801200	7.45755800
C	-2.43471800	3.81749200	8.82782900
H	-3.84431500	2.44425200	7.88563600
H	-1.06166600	5.41967900	9.44169500
N	-2.27892600	3.00434200	9.94261800
H	-2.65152800	2.05604600	9.84432200
C	-1.21603700	3.15237300	10.92160800
H	-1.14749000	4.23826100	11.15301400
N	0.12230500	2.79985500	10.44228300
C	0.47045300	1.57054100	9.88717600
H	0.63811500	3.58760700	10.04346800
C	1.64009800	1.48504900	9.08544200
C	-0.26875300	0.37914300	10.11026100
C	2.05804700	0.27019400	8.54654900
H	2.22530500	2.40081100	8.89031300
C	0.15663200	-0.83301900	9.55978800
H	-1.16904000	0.39228100	10.74245600
C	1.32537300	-0.91831900	8.77281200
H	2.96772300	0.21611300	7.92920100
H	-0.41877300	-1.75399900	9.74034200
C	1.77422100	-2.21084000	8.20820600
N	1.02244100	-3.30332000	8.45529600
N	2.91317700	-2.22125200	7.48490500
C	1.47551900	-4.46149400	7.92869900
C	3.29258000	-3.42399600	7.00258500
N	2.60671600	-4.56892300	7.19935400
C	4.54240900	-3.49036500	6.21442600
C	5.30062000	-2.32593800	5.94902400
C	5.02032600	-4.71794700	5.70612100
C	6.48001300	-2.38970400	5.21068300
H	4.93530400	-1.36232300	6.33577400
C	6.20502700	-4.79490600	4.96939700
H	4.43616100	-5.62882300	5.90854500
C	6.96750100	-3.62587700	4.70635900
H	7.05163800	-1.46626500	5.01149100
H	6.55221500	-5.77713900	4.61604500
N	8.17201600	-3.63965500	4.01060900
H	8.49471800	-2.71025400	3.73100700
C	8.62258700	-4.71314700	3.11821600
H	9.56953600	-4.32895800	2.68779400
N	7.74175200	-5.00448400	2.00003600
H	6.94793000	-5.61241600	2.21772600
C	-1.58637000	2.46082000	12.24134300

C	-0.57761900	2.03031500	13.12604700
C	-2.93471600	2.31934900	12.62681000
C	-0.91005600	1.46033400	14.36410400
H	0.47682600	2.13968300	12.82710800
C	-3.26697600	1.74746800	13.86625800
H	-3.73121400	2.67100200	11.95169500
C	-2.25624600	1.31444300	14.73864600
H	-0.10779000	1.12223000	15.04088200
H	-4.32719300	1.64369000	14.15140500
H	-2.51676400	0.86353000	15.71057000
C	-2.04782600	9.55515700	4.07279900
C	-1.09661400	9.96835300	5.03132300
C	-2.28067900	10.40592300	2.96570700
C	-0.40217500	11.17318900	4.90133200
H	-0.90498200	9.30962200	5.89237300
C	-1.59789400	11.61120600	2.82619300
H	-3.01751900	10.09193800	2.21054100
C	-0.64165800	12.03083800	3.79261700
H	0.33716000	11.44712300	5.67012000
H	-1.79904700	12.26044300	1.95654900
C	0.68479700	-5.68639600	8.16651900
C	1.09193600	-6.93205300	7.63973600
C	-0.50798100	-5.65109200	8.92883300
C	0.35530200	-8.09764600	7.86117300
H	2.01450600	-6.96695100	7.03989700
C	-1.25168400	-6.80491200	9.15783900
H	-0.83686800	-4.68461600	9.34073100
C	-0.84149100	-8.06311100	8.63139100
H	0.70834900	-9.04037000	7.41465700
H	-2.17809700	-6.75240400	9.75614800
N	-0.00763700	13.25124700	3.63687500
H	-0.07851800	13.67853900	2.70947000
N	-1.60196900	-9.18579600	8.87337100
H	-2.46383800	-9.05802700	9.40715500
C	1.14010100	13.68449100	4.41604000
H	0.86963000	13.49476200	5.48657200
C	-1.25182200	-10.55641300	8.47619700
H	-0.95567200	-10.52623100	7.40389300
N	2.34816800	12.97584900	3.98392300
H	3.14198900	13.20834900	4.60058200
H	2.19385500	11.95829700	4.04495900
N	-0.13823600	-11.17109400	9.19164800
H	0.69913100	-10.57229200	9.12955400
H	-0.36632000	-11.26608200	10.19275700
C	7.70219000	-0.08810200	-4.05112000
N	7.89362900	-0.78913500	-2.91265900
C	7.03516400	-1.80673600	-2.69540600
C	5.92272700	-1.39584900	-4.65011000
N	6.73227600	-0.36005100	-4.95114400
N	6.03097600	-2.14406500	-3.53193900

C	7.21009700	-2.61002700	-1.46557300
C	6.32929500	-3.67268800	-1.15380200
C	8.26453900	-2.34321000	-0.56593400
C	6.50087800	-4.43522700	-0.00118300
H	5.49919100	-3.88519500	-1.84473500
C	8.44662100	-3.10243600	0.59259100
H	8.94925400	-1.51279500	-0.79739700
C	7.57205400	-4.17921900	0.89763400
H	5.80128900	-5.25962300	0.22114000
H	9.28540200	-2.85211100	1.26094900
C	4.85130400	-1.73969700	-5.61105200
C	3.95146700	-2.80102300	-5.35481300
C	4.69646400	-1.02104300	-6.81584700
C	2.95012400	-3.13105500	-6.26493300
H	4.05856800	-3.36366400	-4.41484600
C	3.69525500	-1.34338800	-7.73546500
H	5.38842800	-0.18928800	-7.01903500
C	2.80288200	-2.41913400	-7.48599200
H	2.25949400	-3.96324300	-6.04367400
H	3.61933900	-0.75119400	-8.66096800
N	1.83017400	-2.82336000	-8.39165500
H	1.13346000	-3.47375900	-8.01827000
C	1.38745000	-2.02841000	-9.52358800
H	2.30525200	-1.62928700	-10.00893500
N	0.61307600	-0.83379700	-9.17735400
C	-0.54895100	-0.83514300	-8.40951800
H	1.18435200	0.00486200	-9.05053200
C	-0.96497700	0.37312400	-7.78866900
C	-1.36772500	-1.98280500	-8.24102000
C	-2.14533900	0.43606400	-7.05122900
H	-0.33853300	1.27582400	-7.89738100
C	-2.54641500	-1.90967600	-7.49386600
H	-1.09771600	-2.93507900	-8.72120100
C	-2.96480300	-0.70523900	-6.88802800
H	-2.45868600	1.37911100	-6.57787700
H	-3.17910800	-2.80218400	-7.37144900
C	-4.22506800	-0.63669200	-6.11528200
N	-4.95097200	-1.76686000	-5.98967400
N	-4.57903500	0.55417600	-5.58886200
C	-6.10003100	-1.65442600	-5.28947000
C	-5.74506900	0.57341500	-4.90845900
N	-6.53799700	-0.50437100	-4.73436400
C	-6.18411700	1.85963800	-4.32494700
C	-5.39779300	3.02798500	-4.45885100
C	-7.40425300	1.96351800	-3.62203800
C	-5.81657600	4.24133100	-3.91803500
H	-4.44147700	2.95790400	-4.99933400
C	-7.83672000	3.17626700	-3.07940100
H	-8.02133400	1.05851300	-3.51206500
C	-7.05044300	4.35052900	-3.22100500

H	-5.18372000	5.13889700	-4.03222800
H	-8.80668800	3.21437900	-2.56193300
N	-7.44260100	5.59606900	-2.74160400
H	-6.69281500	6.29149200	-2.74214000
C	-8.46398600	5.82742800	-1.71571600
H	-8.43169800	6.92216300	-1.54055800
N	-8.21455900	5.19050800	-0.43296200
H	-8.49970600	4.20979400	-0.36997700
C	0.70037800	-2.90871600	-10.57713500
C	-0.22717300	-2.34778400	-11.47751000
C	1.04477200	-4.26850700	-10.71478800
C	-0.80628400	-3.13223900	-12.48618600
H	-0.49799500	-1.28536400	-11.37202200
C	0.46368000	-5.05378600	-11.72441200
H	1.78403100	-4.71224900	-10.02893500
C	-0.46501400	-4.48921200	-12.61263900
H	-1.53584700	-2.67858600	-13.17750600
H	0.74407800	-6.11629200	-11.81716900
H	-0.92296200	-5.10584300	-13.40376700
C	8.60730300	1.04504000	-4.32757600
C	8.47470000	1.81774000	-5.50287500
C	9.63939300	1.39592700	-3.42382100
C	9.32455400	2.89167600	-5.77545600
H	7.68025900	1.54819400	-6.21586900
C	10.48762600	2.46907200	-3.67892400
H	9.75410700	0.80165200	-2.50428500
C	10.35212100	3.25509000	-4.86016400
H	9.19786800	3.44848600	-6.71633200
H	11.28026200	2.72711000	-2.95509500
C	-6.93051300	-2.86558200	-5.12475000
C	-8.15103100	-2.82467200	-4.41469700
C	-6.53020600	-4.10564700	-5.67811000
C	-8.94778700	-3.96170200	-4.26220200
H	-8.46744600	-1.86480700	-3.97797100
C	-7.31546300	-5.24584800	-5.53299300
H	-5.58043900	-4.14838500	-6.23304900
C	-8.54634300	-5.20773600	-4.81926700
H	-9.88458200	-3.88321800	-3.68837700
H	-6.98428200	-6.20235300	-5.97421100
N	11.21927400	4.30541800	-5.06726400
H	11.84776000	4.54245600	-4.29368400
N	-9.28770000	-6.36441800	-4.67619500
H	-8.98789500	-7.16665000	-5.24022800
C	11.09104700	5.39466000	-6.02447300
H	10.10958100	5.26666700	-6.54108200
C	-10.70910900	-6.40622900	-4.31344600
H	-10.81785200	-5.84499800	-3.35624800
N	11.18500500	6.64428300	-5.25935100
H	11.40501000	7.43377400	-5.88235300
H	10.29210700	6.84650200	-4.78516800

N	-11.64444000	-5.80345300	-5.25344000
H	-11.40842500	-4.81264000	-5.40818200
H	-11.58304200	-6.28776800	-6.16198400
C	-11.08529500	-7.84687600	-4.05255200
C	-10.23257100	-8.86609800	-3.48701000
C	-12.38097100	-8.43535500	-4.28125800
H	-9.18272100	-8.73161000	-3.19341700
C	-11.00040200	-10.07646800	-3.37307600
H	-13.24226400	-7.90343800	-4.70482300
C	-12.32685900	-9.81028400	-3.86540400
H	-10.63322700	-11.03887600	-2.98976800
H	-13.15040000	-10.53556800	-3.92615600
Fe	-10.93323500	-9.45497500	-5.31936400
C	-9.32371600	-9.70593400	-6.56858300
C	-9.97818200	-10.96278500	-6.31578800
C	-10.28678400	-8.81545100	-7.16548800
H	-8.26943700	-9.47679500	-6.35533000
H	-9.51681900	-11.85032100	-5.86069900
C	-11.34456100	-10.84901400	-6.75469700
H	-10.09320400	-7.78625500	-7.50162200
C	-11.53704900	-9.52112900	-7.27584200
H	-12.11092200	-11.63411500	-6.69082600
H	-12.47397700	-9.11753200	-7.68474700
C	12.17699200	5.41124200	-7.08400200
C	12.07490800	6.06606400	-8.36907200
C	13.53910400	4.96347900	-6.93259400
H	11.16231100	6.51009000	-8.79362800
C	13.36352900	6.01001500	-9.00620300
H	13.93694500	4.41237000	-6.06968100
C	14.26740300	5.32777900	-8.11748100
H	13.60807500	6.39751200	-10.00536900
H	15.32333400	5.10057100	-8.32112800
Fe	12.67816600	4.12889200	-8.59083900
C	11.12287100	2.96258200	-9.24756900
C	12.00803500	3.29004300	-10.33407300
C	11.88360600	2.26381400	-8.24574500
H	10.05259200	3.20663800	-9.19241600
H	11.73627200	3.83542800	-11.24877800
C	13.31735700	2.79218300	-10.00361800
H	11.49545100	1.89139800	-7.28761900
C	13.23940000	2.16021700	-8.71307300
H	14.22197500	2.89505800	-10.61935700
H	14.07412300	1.69552800	-8.16991300
C	8.94075400	-5.99519300	3.87697700
C	8.75284400	-7.34930100	3.40802500
C	9.48779900	-6.06590500	5.20915700
H	8.37927700	-7.63866700	2.41666700
C	9.17375000	-8.24562600	4.45273400
H	9.73799800	-5.20086100	5.83742000
C	9.62684300	-7.45201400	5.56386200

H	9.16696800	-9.34332000	4.40072200
H	10.02505300	-7.83607200	6.51328900
H	12.36828100	-4.74141700	3.56619600
C	12.30609800	-5.82871700	3.41521900
C	11.81409700	-6.49629800	2.23863600
C	12.69047100	-6.83517800	4.37029700
H	11.42729000	-6.01140300	1.33064400
C	11.89630300	-7.91544300	2.46608200
H	13.09064700	-6.65108200	5.37712000
C	12.43927600	-8.12440900	3.78221800
H	11.58225400	-8.70022200	1.76379400
H	12.61146700	-9.09771300	4.26275000
Fe	10.71191800	-7.02670600	3.87963500
C	-9.86117500	5.47072500	-2.20691800
C	-10.95800000	4.97653500	-1.40617900
C	-10.32132300	5.56176200	-3.57039800
H	-10.93873400	4.82184200	-0.31903900
C	-12.08222500	4.75549000	-2.27745100
H	-9.71614500	5.90158400	-4.42112700
C	-11.68732600	5.11607800	-3.61304900
H	-13.07310000	4.39271200	-1.97045600
H	-12.32245700	5.07458500	-4.50881200
H	-9.98054500	9.05769500	-2.87437100
C	-10.93917000	8.67785500	-2.49275500
C	-11.23420800	8.33641300	-1.12585500
C	-12.11655900	8.42022000	-3.28012600
H	-10.54057500	8.40446700	-0.27530700
C	-12.59457200	7.86904900	-1.06845400
H	-12.21174300	8.56304800	-4.36559900
C	-13.13981900	7.92252400	-2.39909100
H	-13.11803100	7.51686900	-0.16863300
H	-14.15310200	7.61631500	-2.69466600
Fe	-11.48864600	6.71097100	-2.34429700
C	1.30695200	15.19624000	4.26224100
C	0.48173500	16.06796100	5.00068700
C	2.23730900	15.73669900	3.35522000
C	0.58743200	17.45704600	4.83947300
H	-0.25351800	15.64795900	5.70869400
C	2.34516000	17.12893200	3.19407400
H	2.87681700	15.04443800	2.78415500
C	1.52162800	17.99165600	3.93429600
H	-0.06136400	18.12893000	5.42582300
H	3.07996900	17.54235100	2.48285400
H	1.60747900	19.08398400	3.80893500
C	-2.49275500	-11.43121400	8.60172800
C	-3.14081100	-11.58108700	9.84659000
C	-3.00808400	-12.11887500	7.48699100
C	-4.27683600	-12.39655600	9.97141200
H	-2.75523500	-11.05905800	10.74062800
C	-4.14331700	-12.93576400	7.60841100

H	-2.50964800	-12.01292800	6.50868200
C	-4.78181600	-13.07665400	8.85124700
H	-4.76931400	-12.50284100	10.95232400
H	-4.53259000	-13.46608400	6.72348200
H	-5.67376900	-13.71758400	8.94771600
Zero-point correction =			2.504931 (Hartree/Particle)
Thermal correction to Energy =			2.666607
Thermal correction to Enthalpy =			2.667552
Thermal correction to Gibbs Free Energy =			2.260295
Sum of electronic and zero-point Energies =			-12593.363526
Sum of electronic and thermal Energies =			-12593.201849
Sum of electronic and thermal Enthalpies =			-12593.200905
Sum of electronic and thermal Free Energies =			-12593.608161
HF= -12595.8684566			
Fe-Rb-POP			
0 1			
C	-1.27558000	-2.43690500	0.77230200
C	-0.89866700	-3.87578600	0.38508600
C	-1.04653600	-4.97763700	1.24664400
C	-0.44626600	-4.13479100	-0.92838800
C	-0.74718700	-6.28643400	0.83690600
H	-1.39319100	-4.81747600	2.27999800
C	-0.15552100	-5.43242500	-1.35446900
H	-0.33153400	-3.29848800	-1.63780700
C	-0.30317500	-6.54466700	-0.48207100
H	-0.81909800	-7.10823400	1.56296800
H	0.16925200	-5.60348700	-2.39555500
C	-2.54668600	-2.04113600	-0.00461300
C	-3.69618100	-2.85637500	0.04396300
C	-2.62449500	-0.86349800	-0.77011300
C	-4.88326400	-2.50613900	-0.61226800
H	-3.66487400	-3.80370800	0.60778500
C	-3.80367900	-0.50150900	-1.43421900
H	-1.74282200	-0.21127600	-0.85889800
C	-4.96458200	-1.30781000	-1.36774800
H	-5.74379200	-3.18991800	-0.56150800
H	-3.83002400	0.43658300	-2.01581900
C	-1.43729500	-2.23893200	2.28800100
C	-0.32693500	-2.47784600	3.12930800
C	-2.61284400	-1.75622100	2.89978500
C	-0.37843200	-2.26278900	4.51025600
H	0.61666900	-2.83719700	2.68659800
C	-2.68173200	-1.54061300	4.28090400
H	-3.49902800	-1.53798500	2.28396500
C	-1.56998200	-1.79607700	5.12194000
H	0.52734700	-2.44538500	5.10708700
H	-3.62012400	-1.16440700	4.72468400

O	-0.14955900	-1.59916500	0.35774300
H	-0.12667200	-0.83238500	0.97273700
N	-6.12315500	-0.91880200	-2.05628600
N	-1.68880500	-1.60552000	6.49328800
C	-7.47264800	-1.18800800	-1.52809000
H	-8.14191200	-0.56901900	-2.15715500
N	-7.68024900	-0.76588300	-0.14129200
C	-0.60543100	-1.66907100	7.46009800
H	-0.01243900	-2.58537600	7.24325900
C	-1.20573200	-1.82354200	8.86530300
C	-0.65776900	-1.13797200	9.96521300
C	-2.29652400	-2.69298000	9.08034600
C	-1.19359300	-1.30759600	11.25260300
H	0.19903600	-0.46725500	9.79366300
C	-2.83063400	-2.86471500	10.36686900
H	-2.72694600	-3.24458000	8.22820200
C	-2.28222200	-2.16979400	11.45798300
H	-0.75417100	-0.75956800	12.10282900
H	-3.68177600	-3.54958600	10.51808300
H	-2.70289100	-2.30297600	12.46860000
C	-7.71151000	0.60494200	0.17452700
C	-6.95311600	1.11619700	1.25359200
C	-8.53436800	1.51185200	-0.53596100
C	-7.01217100	2.47096500	1.60329700
H	-6.29259700	0.43396500	1.81726300
C	-8.58605000	2.86602400	-0.17829000
H	-9.17471400	1.14879100	-1.35698900
C	-7.82343600	3.37683100	0.89285700
H	-6.41054400	2.85363700	2.44245000
H	-9.26218100	3.53620200	-0.73467800
C	-7.81456600	4.87339900	1.26988900
C	-6.76854300	5.63205600	0.43382800
C	-9.21963900	5.49640200	1.13968700
O	-7.39915200	5.01893100	2.64626600
C	-6.63151400	5.43126700	-0.95550900
C	-5.94828100	6.60973400	1.02709900
C	-9.44428200	6.78336400	0.61082500
C	-10.33821300	4.81259900	1.66964300
H	-8.19231500	4.82078800	3.19048600
C	-5.73759100	6.18890200	-1.71653800
H	-7.23392300	4.66191700	-1.46374600
C	-5.04351400	7.37537600	0.27487900
H	-6.03036600	6.77692400	2.11101500
C	-10.71867200	7.36334300	0.60861900
H	-8.59957400	7.34838800	0.18618400
C	-11.61526700	5.38350200	1.68071200
H	-10.21242000	3.79280800	2.07341600
C	-4.92954200	7.19280300	-1.12457000
H	-5.65929000	6.00615500	-2.80283800
H	-4.44406300	8.14224500	0.78803700

C	-11.83454600	6.67816300	1.14772800
H	-10.85703500	8.37252900	0.18339100
H	-12.46442600	4.81789900	2.10191200
N	-0.05016700	-7.82372600	-0.95450800
H	-7.06804000	-1.29265800	0.49430800
H	-6.04716400	0.03932600	-2.41135600
H	-2.55016600	-1.16112900	6.81958200
C	-0.16911700	-9.03507600	-0.17660300
H	-1.14910700	-8.99258900	0.36053500
N	0.84921700	-9.12480600	0.87477800
H	0.61017200	-9.86325000	1.55279000
H	1.76187300	-9.36691500	0.45785300
H	0.46646700	-7.91193400	-1.83277900
N	-4.10777700	7.96938500	-1.94519500
N	0.33208000	-0.55046600	7.37229200
C	1.59081000	-0.62751400	6.76630200
H	-0.13897900	0.34966700	7.23800800
C	2.39897600	-1.78629900	6.84102600
C	2.10554200	0.49083600	6.06288300
C	3.63499600	-1.84031300	6.17528400
H	2.07686800	-2.65382300	7.43958100
C	3.34328200	0.43048000	5.41980500
H	1.50220200	1.41372000	6.00239700
C	4.12376300	-0.74547200	5.44277300
H	4.23527100	-2.76184800	6.24282400
H	3.71465200	1.30730100	4.86682300
C	5.42736900	-0.78851400	4.63223100
C	5.09565800	-0.91635000	3.12780800
C	6.36910400	-1.90844800	5.10953500
O	6.07392800	0.47921400	4.89192000
C	5.85536700	-0.22444500	2.16320600
C	4.04806500	-1.72983200	2.65172300
C	6.99191900	-1.77395400	6.37205300
C	6.66147400	-3.06633200	4.36277000
H	7.01245100	0.37069100	4.62363700
C	5.60276500	-0.36031100	0.79582700
H	6.65469700	0.46165200	2.48553300
C	3.77652500	-1.87430400	1.28204700
H	3.40552900	-2.26153400	3.37345000
C	7.86334800	-2.74755100	6.86757900
H	6.78420900	-0.87393500	6.97342200
C	7.53255400	-4.05065000	4.85005100
H	6.20279300	-3.20367900	3.37079500
C	4.56905100	-1.20517900	0.31713200
H	6.21720800	0.20109300	0.07026300
H	2.92525400	-2.50122200	0.97333700
C	8.15195500	-3.91459500	6.11508000
H	8.33055700	-2.61199600	7.85863100
H	7.74082700	-4.94520000	4.23781000
N	4.41537800	-1.36561100	-1.05780000

C	3.23636600	-1.91834800	-1.70597100
H	4.89859200	-0.65487300	-1.61339900
N	2.04097000	-1.07183600	-1.67783200
H	2.94419900	-2.82697100	-1.14105000
C	2.02864400	0.25912300	-2.07390200
H	1.33807200	-1.32829900	-0.96906000
C	2.98983100	0.81501900	-2.96319200
C	1.01656300	1.13054600	-1.59631700
C	2.95309700	2.17104100	-3.30098800
H	3.76117000	0.17496900	-3.41824100
C	0.98175600	2.48354100	-1.95727800
H	0.24994100	0.72755100	-0.91473700
C	1.96541800	3.04591900	-2.79515300
H	3.71328800	2.57273700	-3.99078900
H	0.17037000	3.11390700	-1.56064100
C	1.98519200	4.50837300	-3.26866100
C	3.35082500	5.17288500	-3.02131000
C	0.90335400	5.39166700	-2.60665600
O	1.80699100	4.50204100	-4.70262800
C	4.14071900	4.87069100	-1.89736300
C	3.82856700	6.16165400	-3.90789300
C	-0.01465200	6.11170100	-3.38838900
C	0.83190200	5.56959900	-1.20608700
H	1.05684100	3.89173700	-4.87636500
C	5.35695700	5.52602100	-1.64968100
H	3.81645000	4.08052200	-1.20001100
C	5.03495700	6.82519100	-3.67349500
H	3.23596100	6.40952000	-4.80170700
C	-0.97223300	6.96597200	-2.81716900
H	0.03215600	6.00905800	-4.48362100
C	-0.11854300	6.41041800	-0.62310000
H	1.54657500	5.04662700	-0.54967800
C	5.82793700	6.53143400	-2.53222500
H	5.95983500	5.22311200	-0.77949000
H	5.38234200	7.59547400	-4.38439700
C	-1.04093100	7.14258200	-1.41568400
H	-1.66202000	7.50012800	-3.48968600
H	-0.13954800	6.53126500	0.47403400
N	7.02709100	7.19746600	-2.32891900
N	-1.92049400	8.02853600	-0.79280600
C	7.69247100	7.32462500	-1.03080900
H	7.21478100	8.00695000	-2.92615300
C	-2.96216000	8.75841100	-1.48578600
H	-2.08236300	7.86031700	0.20310800
H	6.90482100	7.19030100	-0.24331600
N	8.28057700	8.65740200	-0.94298800
H	-2.50121500	9.13616200	-2.42650900
C	-3.38061000	10.00560000	-0.69186400
H	7.75209600	9.28326200	-0.32408400
H	9.26235600	8.61245200	-0.64347300

C	-2.48075700	10.63634000	0.19066600
C	-4.64787800	10.58718400	-0.89724500
C	-2.84487300	11.81541900	0.86241300
H	-1.47987800	10.20178700	0.34196300
C	-5.01066000	11.76560500	-0.22807300
H	-5.35171700	10.09616800	-1.58770100
C	-4.11159900	12.38394100	0.65704700
H	-2.12755400	12.29436100	1.54978600
H	-6.00894400	12.20301100	-0.39688500
H	-4.39846500	13.30844300	1.18530700
H	-3.98120100	7.57278900	-2.87892400
N	-13.08897200	7.27024900	1.19461500
H	-13.89300600	6.64977400	1.31243000
H	-13.25740800	8.05346700	0.55934600
N	8.97570000	-4.90971600	6.62526100
H	9.37795200	-5.56729900	5.95340400
H	9.61592700	-4.64134700	7.37601500
C	8.72870900	6.23897700	-0.79694600
C	9.64223500	6.16573400	0.32185700
C	8.92734300	5.05624200	-1.59660500
Fe	10.66801000	6.11983600	-1.44624300
C	10.39903300	4.94753000	0.20628000
H	9.73945800	6.90758500	1.12788500
C	9.95584000	4.26225000	-0.97992600
H	8.38593100	4.82861700	-2.52410600
C	10.99723400	7.68620700	-2.73094900
H	11.18498800	4.60793700	0.89567300
H	10.34848800	3.30809600	-1.35873300
C	11.83634600	7.80180500	-1.56564400
C	11.29489500	6.43049700	-3.36779200
H	10.24435200	8.41698600	-3.05646200
C	12.65206500	6.61804400	-1.48278900
H	11.86166800	8.64914400	-0.86505700
C	12.31877400	5.77166000	-2.59888300
H	10.81230800	6.03706400	-4.27332200
H	13.39438000	6.39751200	-0.70287700
H	12.75786100	4.78801800	-2.81722100
C	3.60795800	-2.34556400	-3.12490700
C	2.66935400	-2.71383900	-4.15402900
C	4.93277200	-2.42938800	-3.69678700
Fe	4.00048400	-4.23849700	-3.82485500
C	3.40494000	-3.01427800	-5.35240800
H	1.57829600	-2.74434100	-4.03136900
C	4.80494900	-2.83624600	-5.07168500
H	5.87316500	-2.24376800	-3.16124800
C	4.76180800	-5.47118400	-2.37701000
H	2.97331600	-3.33585800	-6.31056600
H	5.63334000	-3.00068700	-5.77504900
C	3.33151100	-5.60968500	-2.45868900
C	5.31659700	-5.79871800	-3.66451700

H	5.32787600	-5.14664500	-1.49252300
C	3.00258400	-6.01977500	-3.80094200
H	2.61251400	-5.41136400	-1.65004500
C	4.22993700	-6.13960300	-4.54471500
H	6.38173300	-5.77428200	-3.93409400
H	1.99084100	-6.18672400	-4.19888100
H	4.31959200	-6.42380500	-5.60255400
C	-7.87510500	-2.64453400	-1.70201300
C	-7.53909300	-3.48137800	-2.82706400
C	-8.65454500	-3.43869800	-0.78235900
Fe	-9.57091100	-3.36564800	-2.60786700
C	-8.09793200	-4.78647700	-2.59795800
H	-6.94546200	-3.16428700	-3.69471700
C	-8.78776300	-4.76089700	-1.33493000
H	-9.07961800	-3.07417100	0.16182200
C	-10.35526600	-1.99054100	-3.90511600
H	-8.02430800	-5.64718000	-3.27734700
H	-9.33671200	-5.59751000	-0.88035700
C	-10.50735600	-3.32381800	-4.42713400
C	-11.03012300	-1.93022800	-2.63504000
H	-9.80774400	-1.16878400	-4.38888600
C	-11.27799400	-4.08633500	-3.48042900
H	-10.09342000	-3.69761600	-5.37408500
C	-11.59936300	-3.22619700	-2.37213600
H	-11.08526000	-1.05650500	-1.96955500
H	-11.55409800	-5.14576000	-3.57710600
H	-12.16459900	-3.51217500	-1.47411300
C	-0.23142900	-10.22357600	-1.12288100
C	0.20217600	-11.56627600	-0.81671300
C	-0.81977900	-10.25243600	-2.44234500
Fe	1.12906500	-10.89122400	-2.50549100
C	-0.11045100	-12.41127000	-1.93783900
H	0.70044100	-11.88240400	0.11014000
C	-0.74026100	-11.59744100	-2.94413200
H	-1.25607600	-9.39034800	-2.96493400
C	3.14210000	-10.87716100	-2.11717300
H	0.11024700	-13.48496100	-2.01786300
H	-1.08665000	-11.94105400	-3.92915800
C	2.82104700	-11.84840500	-3.13010500
C	2.72191800	-9.58396700	-2.58964000
H	3.62927100	-11.08803000	-1.15458600
C	2.19639000	-11.15624800	-4.22735000
H	3.00934800	-12.92961600	-3.07129000
C	2.13338800	-9.75827300	-3.89180400
H	2.85545200	-8.62518800	-2.06791600
H	1.82452600	-11.61602400	-5.15372000
H	1.71816100	-8.96002800	-4.52277200
Zero-point correction =			2.202510 (Hartree/Particle)
Thermal correction to Energy =			2.341599

Thermal correction to Enthalpy =	2.342544
Thermal correction to Gibbs Free Energy =	1.996116
Sum of electronic and zero-point Energies =	-11285.954002
Sum of electronic and thermal Energies =	-11285.814913
Sum of electronic and thermal Enthalpies =	-11285.813968
Sum of electronic and thermal Free Energies =	-11286.160396
HF=	-11288.1565121

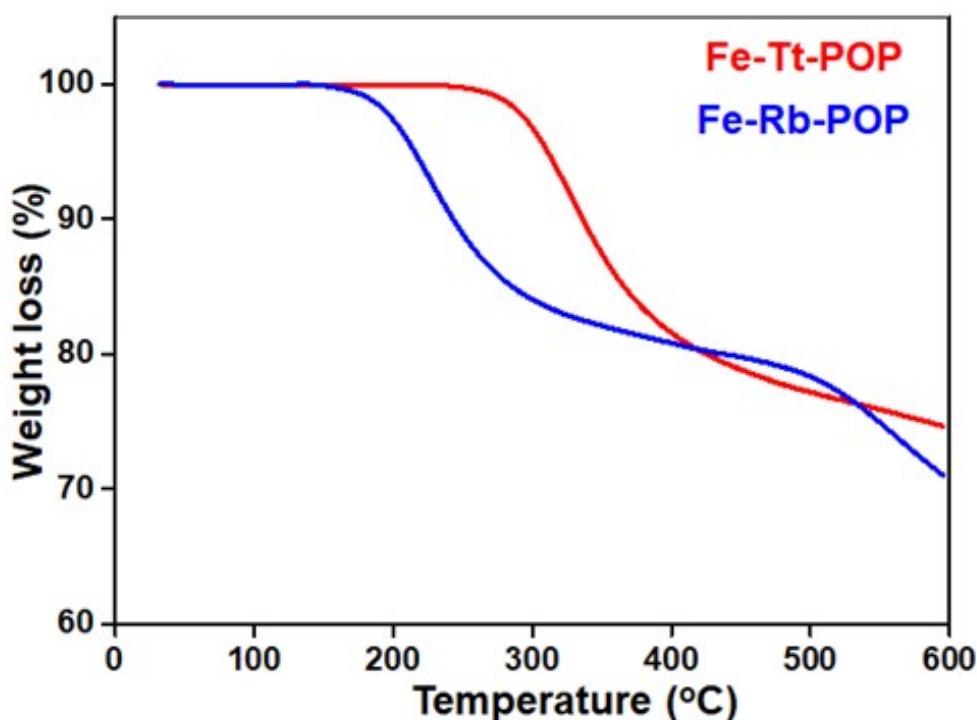


Figure S1: Thermo Gravimetric Analysis (TGA) of **Fe-Rb-POP** & **Fe-Tt-POP**.

In case of **Fe-Rb-POP**, almost 20% weight loss was experienced in the range of 200 to 300°C, demonstrating the fragmentation of hydroxyl functional groups of polymeric networks in the form of small molecules such as CO₂ or H₂. Interestingly, overall, 30% weight loss up to 600°C clearly confirms the convenient thermal stability of **Fe-Rb-POP**. However, **Fe-Tt-POP** exhibited superior thermal stability compared to **Fe-Rb-POP** with gradual drop of ~20 % weight from 350°C to 420°C due to the functional group decomposition to the small molecules (**Figure S1**). No further prominent weight loss with continuous heating illustrates superb thermal as well as mechanical stability of our **Fe-Rb-POP** catalyst.

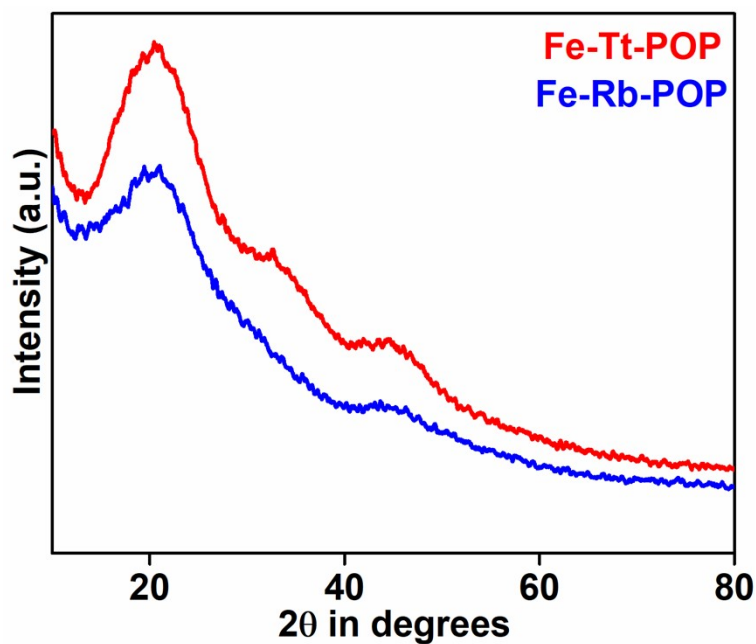


Figure S2: Wide angle PXRD patterns of the respective **Fe-POPs**.

The wide angle PXRD patterns of the **Fe-POPs** exhibited a broad peak between of $2\theta = 15^\circ$ to 25° , which indicated the amorphous nature of the as-synthesized **Fe-POPs**. The absence of any sharp peaks clearly demonstrates that no metal oxides has been formed during the synthesis procedure and the ferrocene core has been intact in the polymeric framework.

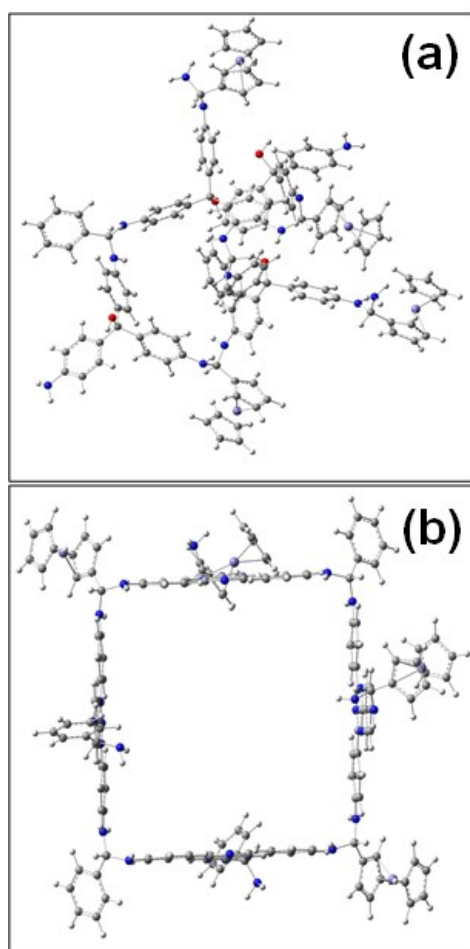


Figure S3: Optimized geometry of the **Fe-Rb-POP** (a) and **Fe-Tt-POP** (b) systems, respectively.

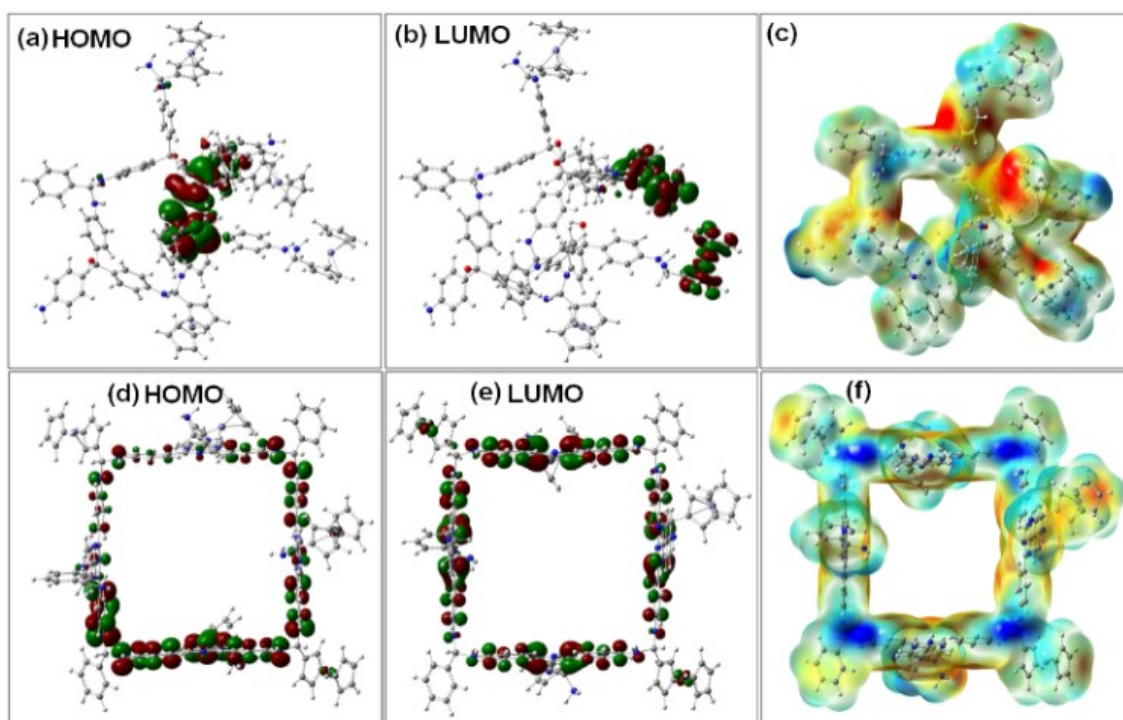


Figure S4: (a & d) HOMO; (b & e) LUMO, and (c & f) ESP maps of **Fe-Rb-POP** and **Fe-Tt-POP**, respectively. All calculations are performed in the gas phase at the B3LYP/Def2-SV(P) level of theory. Iso-value of ESP map is 0.0004. Iso-value of the orbitals is 0.02.

The structural and electronic properties of **Fe-POPs** are shown in the **Figure S4**. The optimized geometry of the POP display a pore size varied from about 10 to 14 Å (**Figure S3, SI**). The Electrostatic Potential (ESP) maps show that the most negative charges are found at the tris(4-aminophenyl)-methanol moieties whereas the most positive charges are found at amine groups of the compound (**Figure S4c**). Moreover, the Highest Occupied Molecular Orbital (HOMO) is locally distributed at some aniline groups (**Figure S4a**) whereas the Lowest unoccupied Molecular Orbital (LUMO) distributions are only found at the ferrocenyl moieties (**Figure S4b**). This observation suggests the reactive zones of **Fe-Rb-POP** compound in the reactions with the external adsorbate compounds. While **Figures S4d to S4e** represent the optimized geometry, the HOMO and the LUMO distributions as well as the ESP maps calculated in the gas phase for the **Fe-Tt-POP** structure. The geometrical properties calculation shows that the pore size of one POP unit is about 15 Å with a square shape (**Figure S3b, SI**). Both the HOMO and LUMO distribute along the four edges of the POP unit (**Figures S4d & S4e**). It is worth noting that the frontier orbitals are not found at the ferrocenyl moieties. Thus, In addition, the ESP maps calculation (**Figure S4f**) shows that the most negative charged zones with the red color are found at the aromatic rings distributed

along the four edges of the pore, whereas the four corners display the most positive charges with blue color.

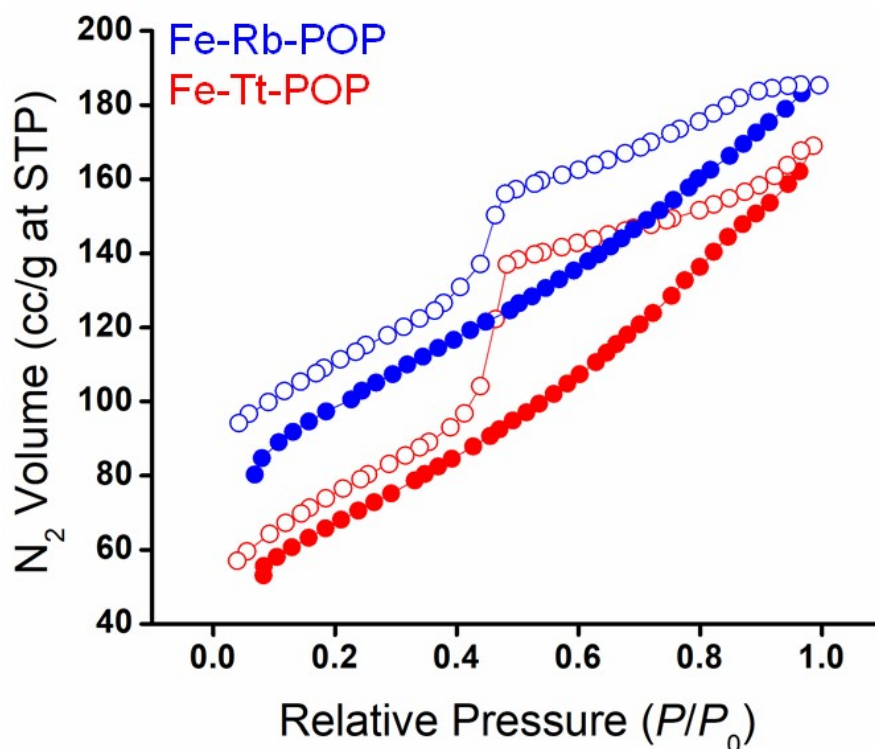


Figure S5: N₂-adsorption/desorption isotherms as measured at 77 K of the respective Fe-POPs.

Both the Fe-POPs comprises typical type IV isotherms with gradual N₂ uptake and a large H₃-type hysteresis loop at high P/P_0 (0.4-0.8) region which is characteristic feature of the mesoporous materials. Generally large hysteresis loop is reflected in the POP based materials owing to their flexible elastic expansion of restricted access pores (nominally closed pores) and swelling of polymeric framework leading to irreversible gas uptake during gas adsorption.

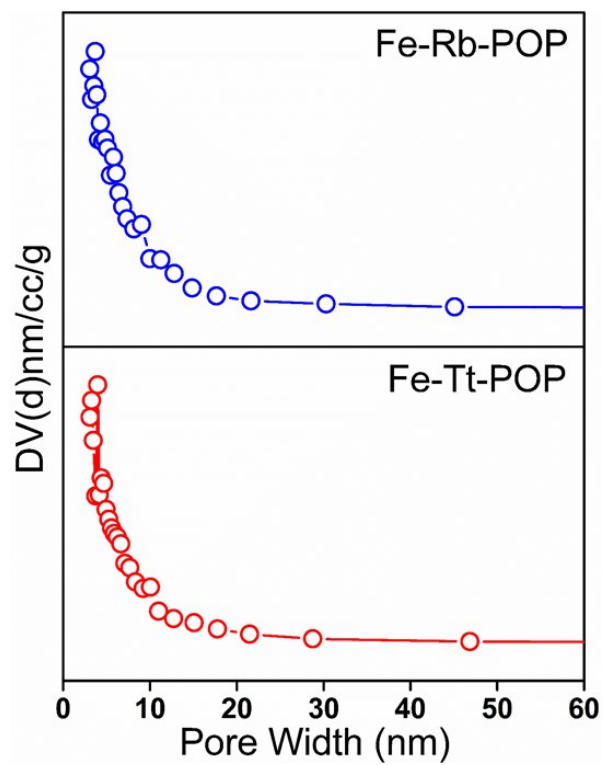


Figure S6: Pore-size distributions of the respective **Fe-POPs** as calculated by NLDFT method.

Comparison between ternary copolymerization and binary co-polymerized approaches:

Specifically ternary copolymerization synthetic strategy is a promising pathway to modulate the porosity, intermolecular aggregation as well as solubility of the final porous polymer by modifying the chemical nature and the relative amount of the monomers.^{9,10} Zhou and co-workers reported that porous materials obtained from ternary co-polymerization exhibited higher cross-linking, greater number of acid groups and active centres compare to binary counterpart. The significant difference was noticed N_2 adsorption-desorption method, whereas binary copolymerized material MPD-[C₄V]-[SO₃CF₃] attributed nonporous feature of the surface due the spherical close packing with comparatively small specific surface area of 46.35 m²g⁻¹, led to lower gas adsorption on their surface. However, MPD-[C₄V]-[VBIM][SO₃CF₃] material synthesized through the ternary copolymerization between divinylbenzene, 1-vinylimidazole, and 1-vinyl-3-butylimidazolium bromide, exhibited the appearance of typical IV isotherm with obvious H1-type hysteresis loop, illustrate the presence of mesopores and macropores in the sample surface. It also manifested in higher surface area (89.47 m²g⁻¹) and larger pore volume (0.29 cm³/g) of MPD-[C₄V]-[VBIM][SO₃CF₃]. Almost two-fold rise on surface area and formation of pores in case of ternary copolymerization approach increased the possibility of the interaction between the reagent and the active site and also facilitate the mass transfer through the porous channels.¹¹ Similar trend was noticed by Chen and co-worked during the development of aminal-linked polymers through binary and ternary co-polymerization. Here, ternary copolymerization significantly increased the surface area 147 m² g⁻¹ (binary polymer Fc-MA POP) to 633 and 756 m²g⁻¹ for Bn-Fc-MA POP and TF-Fc-MA POP, respectively.¹² We have also observed similar kind of trend regarding a diminishment of surface area from 296 m²g⁻¹ to 74 m²g⁻¹ for binary co-polymerization synthetic approach using Fe-CHO & 4,4',4''-(1,3,5-Triazine-2,4,6-triyl) trianiline (Tt) yielding **Fe-Tt-POP-B**. We have conducted N_2 -adsorption-desorption isotherms profile of the binary co-polymerized **Fe-Tt-POP-B** (**Figure S7, SI**). Considering the impressive advantages including higher porosity and excellent catalytic activity of ternary co-polymerization method, we have designed aminal-linked porous polymer using ferrocenealdehyde (Fe-CHO), benzaldehyde (Bn-CHO), 4,4',4''-(1,3,5-Triazine-2,4,6-triyl) trianiline (Tt) rather than the utilisation binary polymerization between ferrocene aldehyde (Fe-CHO) and triamine.

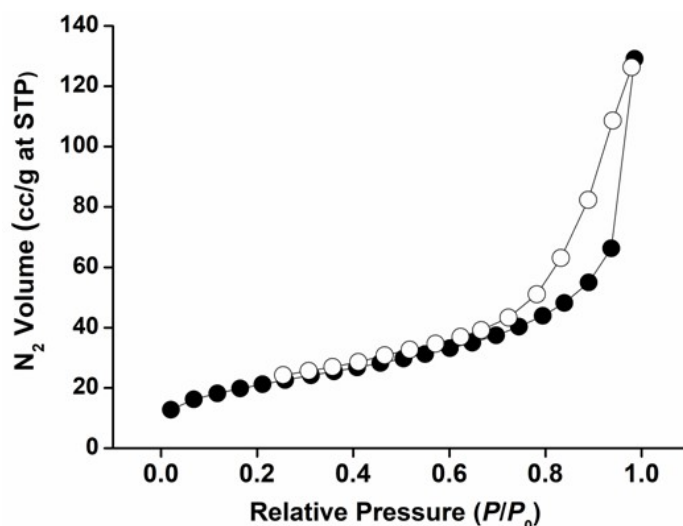


Figure S7: N₂ adsorption-desorption isotherms of the binary copolymerized **Fe-Tt-POP-B** as measured at 77K.

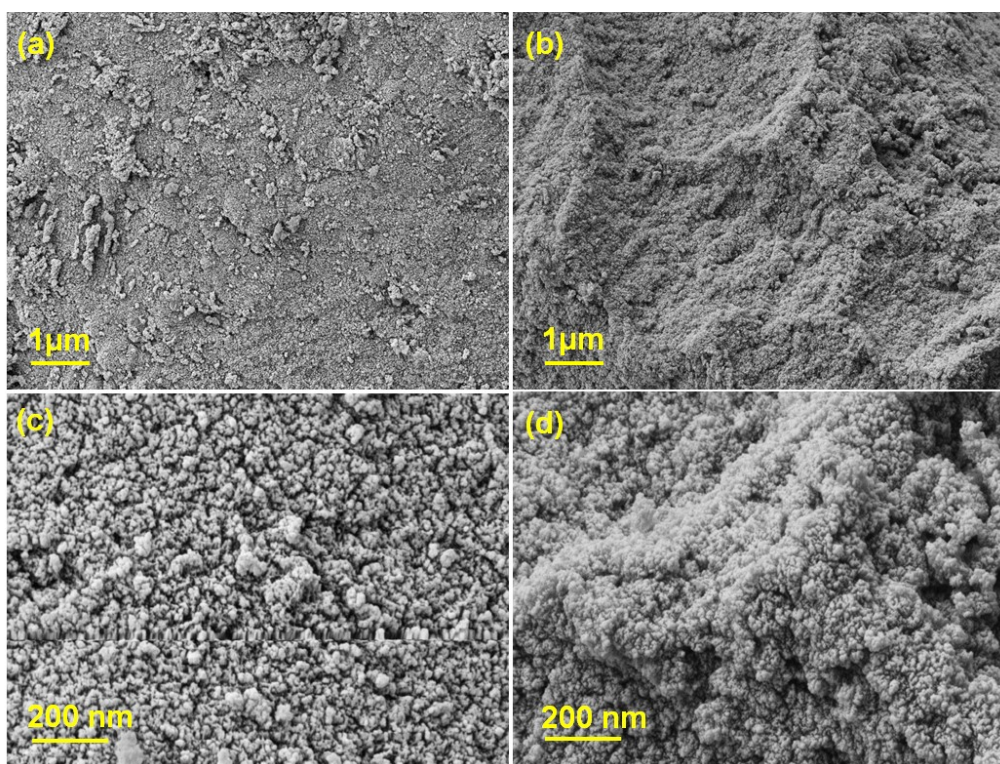


Figure S8: FE-SEM images (a & b) of **Fe-Rb-POP** & (c & d) of **Fe-Tt-POP**, respectively.

Surface morphology as well as microstructure of the as-synthesized **Fe-Rb-POP** & **Fe-Tt-POP** hybrid materials has been illustrated by FE-SEM analysis. We observed a parched-earth type of morphology with the appearance of chunks for the rosoline based porous organic polymer, which is due to the random agglomeration of particles during high temperature synthesis process. In case of **Fe-Tt-POP**, FE-SEM microscopic image reveals the similarity with the satellite image of a hill station, probably accumulation of Fe based porous organic

polymer at high temperature synthesis process could be the reason behind this unique structure with highly rough surface.

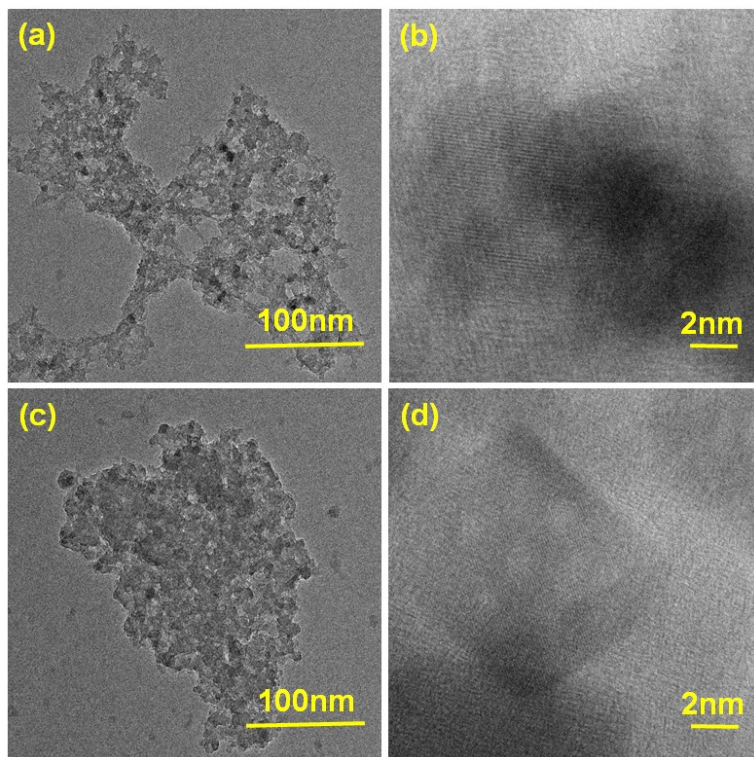


Figure S9: TEM images (a & b) of **Fe-Rb-POP** & (c & d) of **Fe-Tt-POP**, respectively.

On the further inspection of surface morphology through TEM analysis, the surface roughness is clearly recognizable for both catalysts (**Fe-Rb-POP** & **Fe-Tt-POP**), displayed on **Figure S9, SI**.

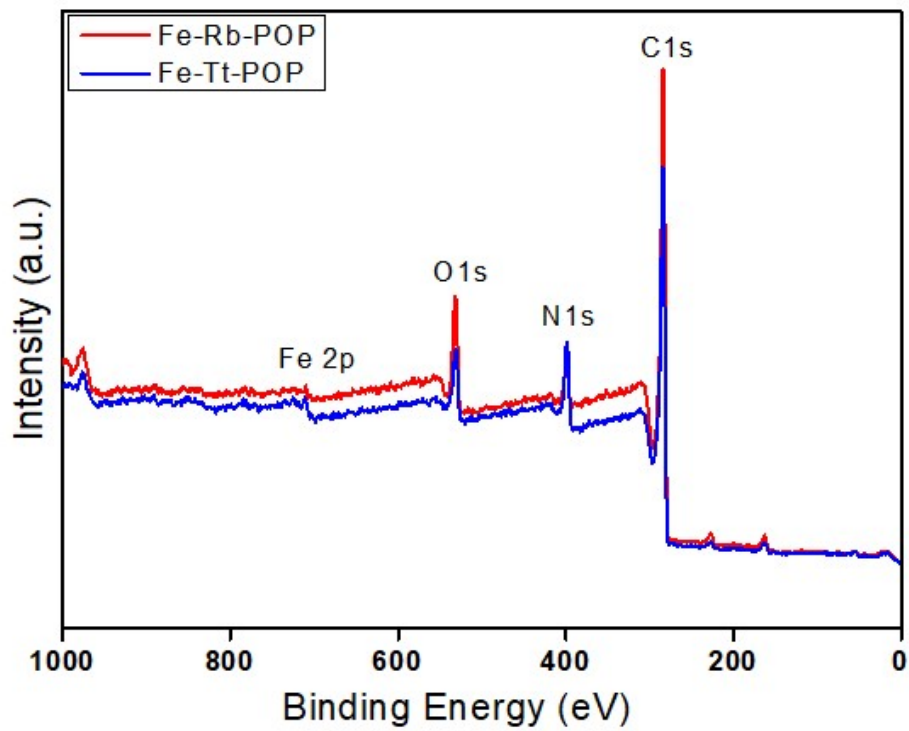


Figure S10: XPS survey spectra of the respective **Fe-POPs**.

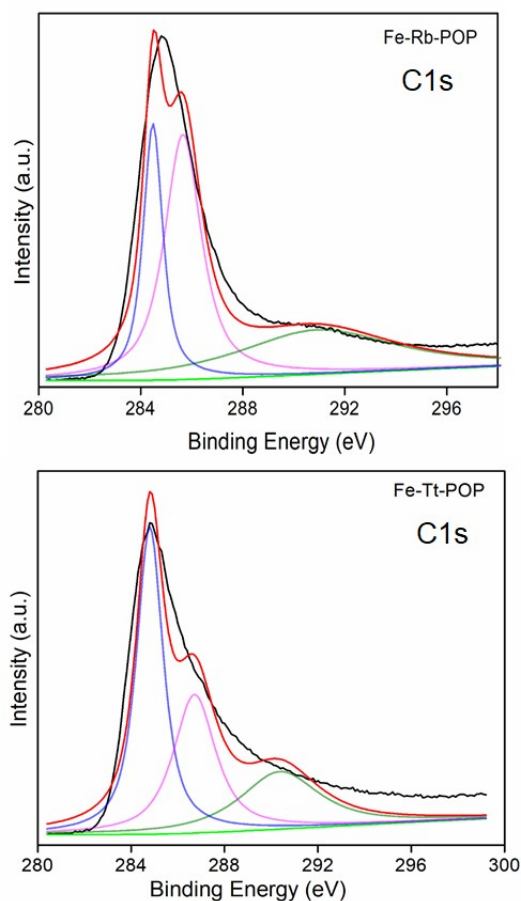


Figure S11: XP-spectra at C-1s core region of the respective **Fe-POPs**.

High resolution C-1s XPS spectra can be deconvoluted into three different types of binding energies, which could be attributed to the (284.4 eV) C-C/C=C, (285.6 eV) C-OH & (290.4 eV) C-N/C=N bonding in the POP frameworks.

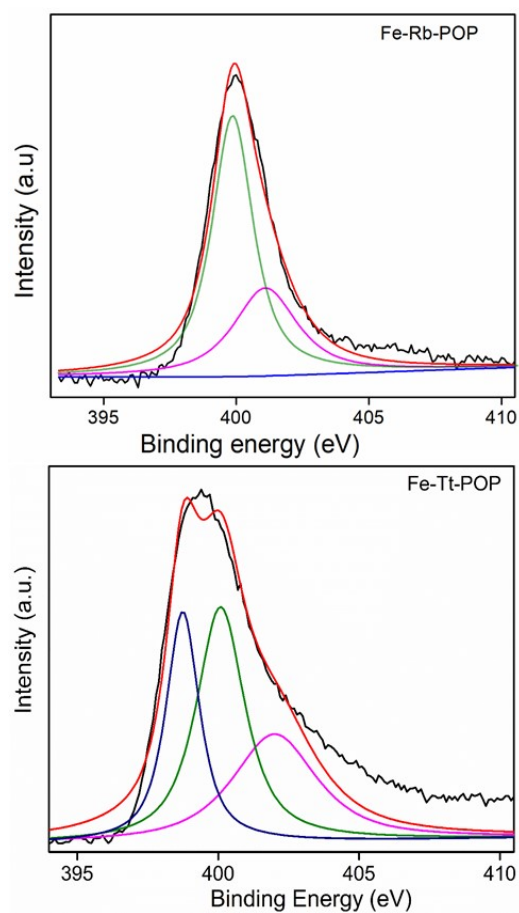


Figure S12: XP-spectra at N-1s core region of the respective **Fe-POPs**.

Deconvoluted N-1s XPS spectrum of **Fe-Rb-POP** appeared at 399.8 eV & 401.0 eV could be assigned to C-N & N-H type of bonds. In the deconvoluted N-1s XPS spectrum of **Fe-Tt-POP**, three distinguishable binding energy peaks located at 398.0 eV, 399.8 eV & 401.0 eV, corresponds to triazine unit, C-N & N-H, respectively.

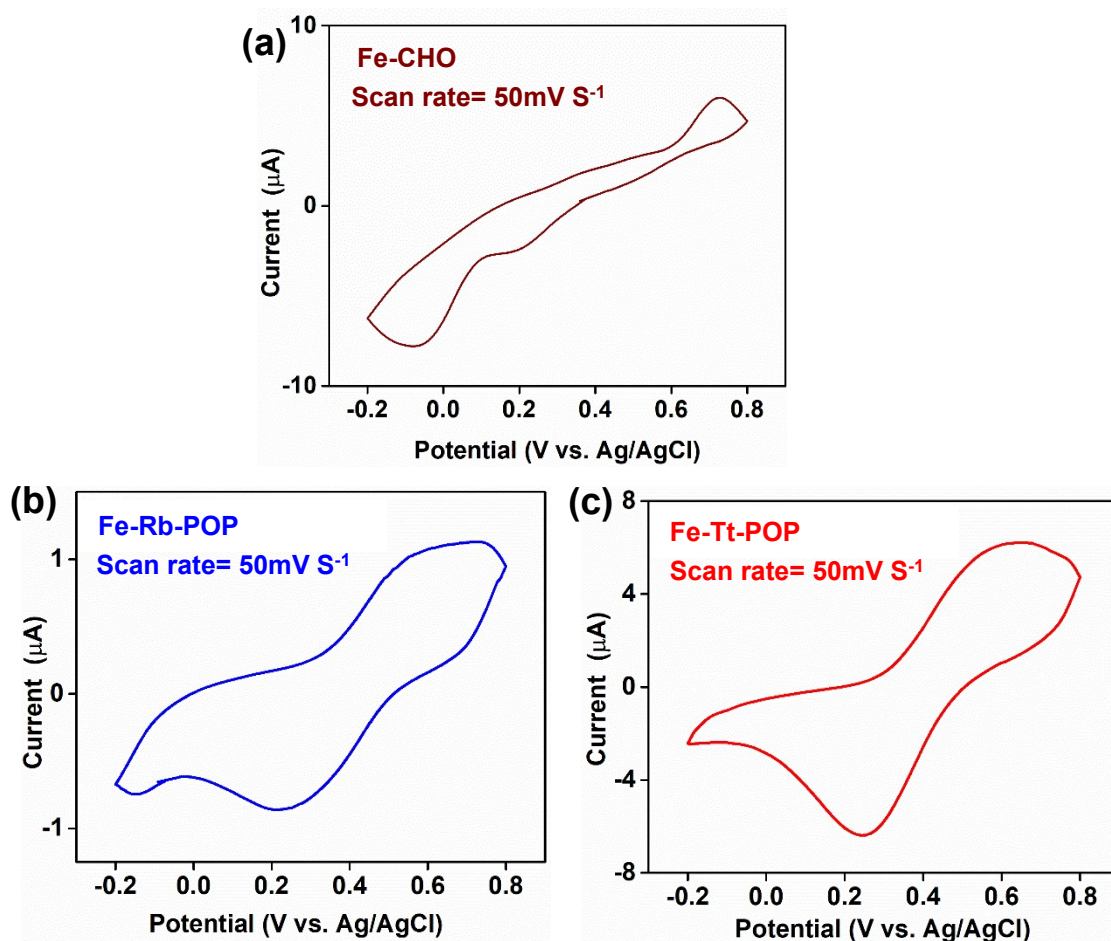


Figure S13: Cyclic Voltammetry (CV) pots of Ferrocene aldehyde (a), **Fe-Rb-POP** (b) and **Fe-Tt-POP** (c), respectively, referenced to saturated calomel electrode (SCE) at a scan rate of 50 mV S^{-1} .

Both the **Fe-POPs** demonstrates CV curves with distinct oxidation and reduction peaks at 0.63 and 0.24 V, respectively. Moreover, at the similar scan rate of 50 mV S^{-1} , the current density of **Fe-Rb-POP** and **Fe-Tt-POP** is 1.14 and 6.23 Ag^{-1} , respectively. The higher current density for **Fe-Tt-POP** clearly indicates the higher conductivity in the planer system compared to the non-planer **Fe-Rb-POP** system.

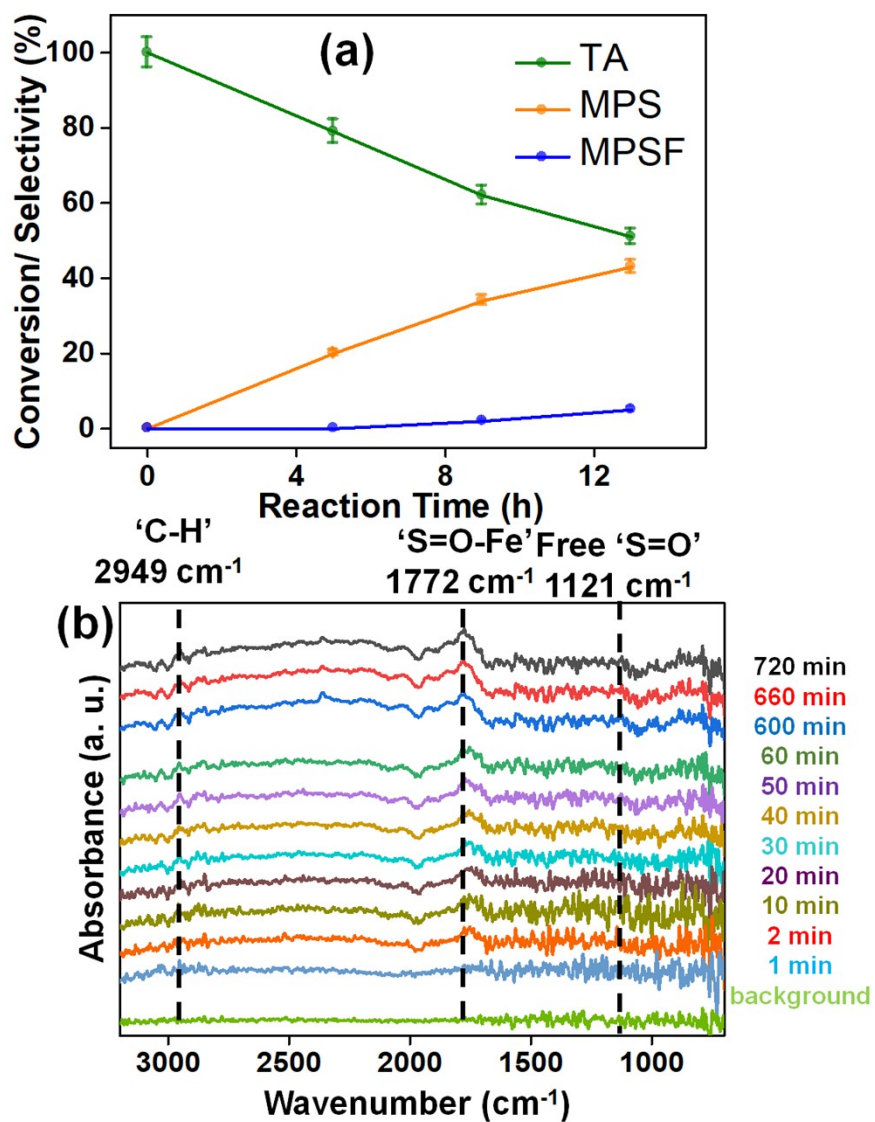


Figure S14: Distribution of reactant and product against time using **Fe-Rb-POP** (a); *In-situ* DRIFTS measurements of **Fe-Rb-POP** (b).

Table S3: The table of product distribution under the influence of different reaction conditions such as without catalyst, without H₂O₂, under N₂ atmosphere, and at room

Entry	Catalyst	100 °C	Variation	Time (hour)	MPS Yield (%)
[1] ^a	Fe-Tt-POP	+	-	13	94%
[2] ^b	Fe-Rb-POP	+	-	13	43%
[3] ^c	Without catalyst	+	-	13	trace
[4] ^d	Fe-Tt-POP	+	No H ₂ O ₂	13	trace
[5] ^d	Fe-Rb-POP	+	No H ₂ O ₂	13	trace
[6] ^e	Fe-Tt-POP	+	N ₂	13	trace
[7] ^e	Fe-Rb-POP	+	N ₂	13	trace
[8] ^f	Fe-Tt-POP	-	Room Temp.	13	trace
[9] ^f	Fe-Rb-POP	-	Room Temp.	13	trace

temperature.

Reaction conditions: TA (0.5 mmol), Fe-POPs (50mg), acetonitrile (20 mL), 100°C, H₂O₂ (0.25 ml). For **Fe-Tt-POP**^a & **Fe-Rb-POP**^b Isolated yield, without using any catalyst^c, without H₂O₂^d, in N₂ atmosphere^e, in room temperature^f.

Similar experiments were carried out under different reaction conditions like without catalyst, without H₂O₂, under N₂ atmosphere, and at room temperature with the best performing **Fe-Tt-POP** catalyst. All the above-mentioned experiments exhibit a very less amount of TA conversion with a trace amount of sulfoxide (MPS) production.

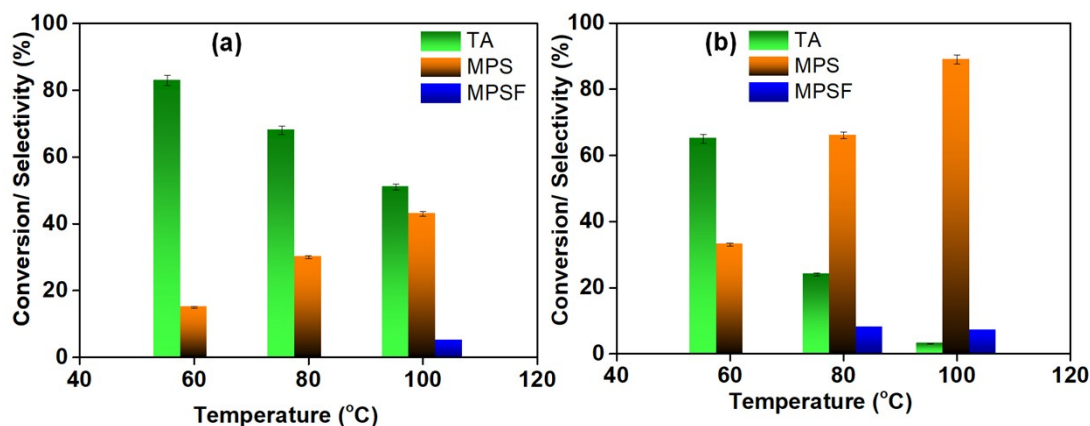


Figure S15: Influence of reaction temperature ($^{\circ}$ C) for catalytic oxidation of TA with **Fe-Rb-POP** (a) & **Fe-Tt-POP** (b), respectively. Reaction Conditions: TA (0.5 mmol), H_2O_2 (0.25 ml) CH_3CN (10 ml), catalyst (50 mg), temperature (100 $^{\circ}$ C), and time (13 h).

We have also performed the catalytic oxidation under various temperatures keeping the other reaction parameters constant for the comparison study. At 60 $^{\circ}$ C, **Fe-Tt-POP** catalyst shows 35% TA conversion with 34% sulfoxide (MPS) selectivity, while **Fe-Rb-POP** shows only 17% conversion with 15% selectivity. With increasing temperature up to 80 $^{\circ}$ C, both the conversion (35 to 76%) and selectivity (33 to 65%) increases for **Fe-Tt-POP**. At 100 $^{\circ}$ C, **Fe-Tt-POP** exhibits maximum catalytic activity with 100% TA conversion, while only 48% conversion was observed in the case of **Fe-Rb-POP**.

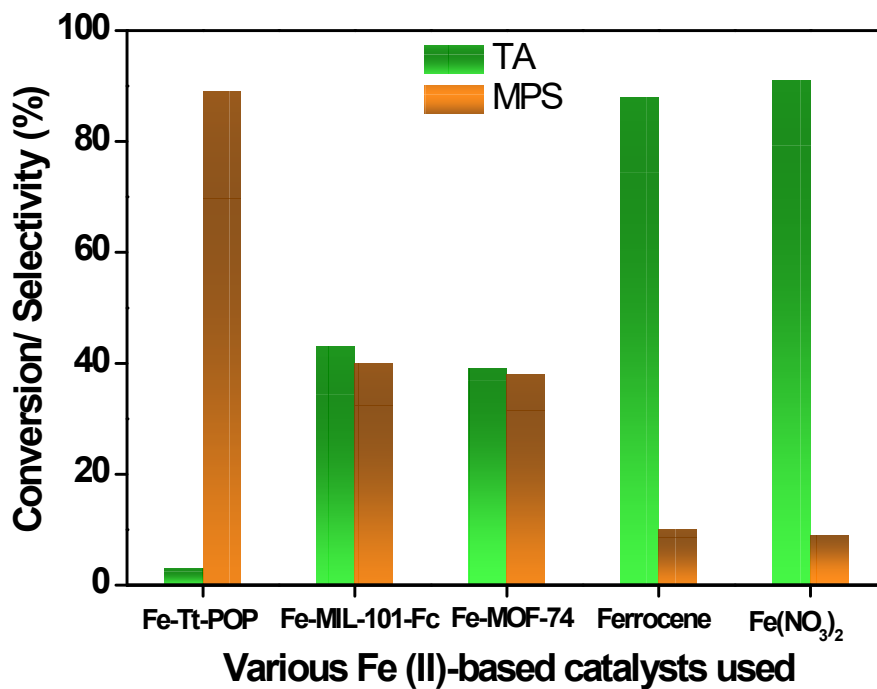


Figure S16: Catalytic property tests with various Fe (II)-based catalysts under optimized reaction conditions.

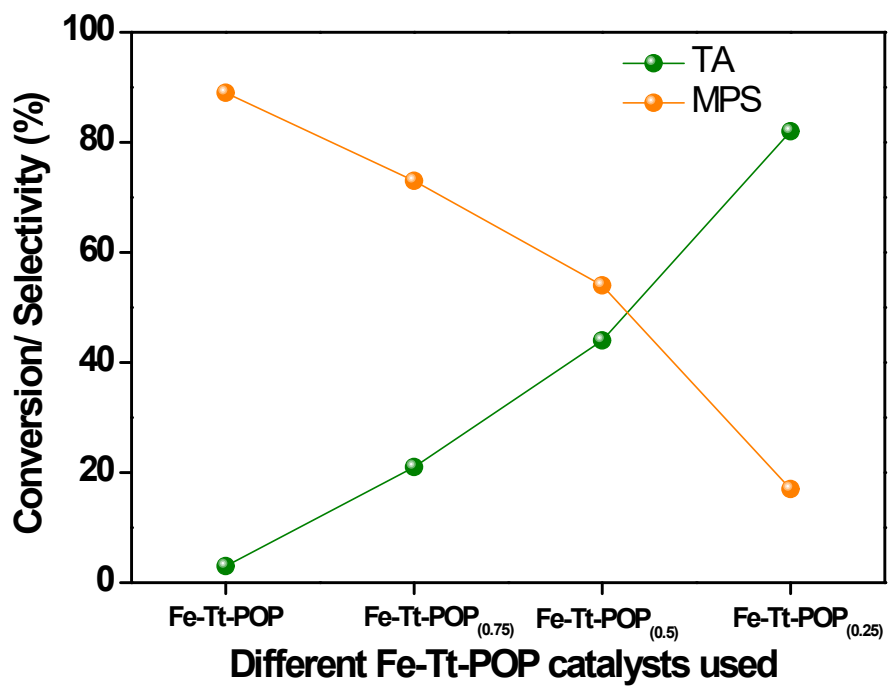


Figure S17: Catalytic property tests with Fe-Tt-POP catalyst with various Fe contents under optimized reaction conditions.

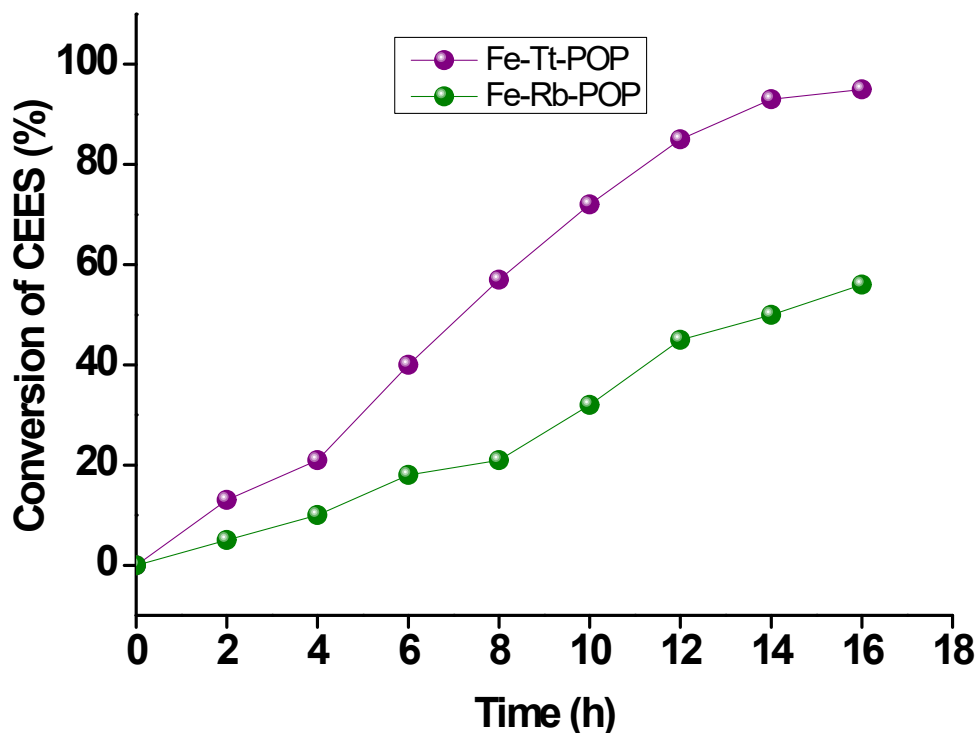


Figure S18: Time profile for the oxidative decontamination of CEES using **Fe-Tt-POP** & **Fe-Rb-POP** catalyst under optimized reaction conditions.

Our as-synthesized **Fe-Tt-POP** catalyst exhibited excellent partial oxidation of sulfur mustard to their corresponding sulfoxide derivatives with almost 95% conversion and more than 78% selectivity for every individual sulfur mustard (**Figure S17**). The conversion of CEES in the time profile diagram was appeared to be poorer when **Fe-Rb-POP** catalyst was used instead of **Fe-Tt-POP** (**Figure S17**), signifying the decisive role of organic polymer back-bone unit arrangement.

Table S4: Comparison study in thioanisole conversion to methyl phenyl sulfoxide with other previous reported catalysts under various reaction conditions.

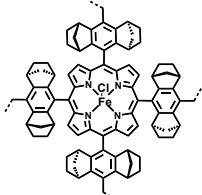
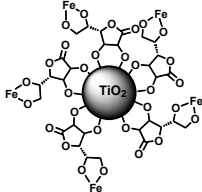
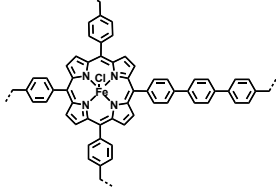
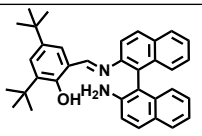
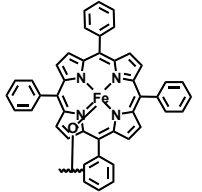
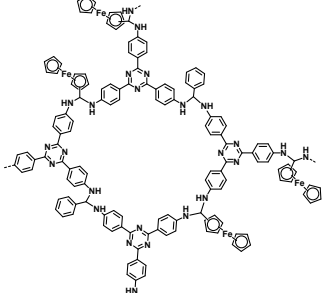
Entry	Previously Reported Catalyst	Conditions	Conversion	Ref.
1		alkene (400 μ mol), PhIO (200 μ mol) and catalyst (1 μ mol) CH ₂ Cl ₂ (1 ml) 5 h, Substrate 0.5 mmol	43%	[13]
2		sulfide/TBHP/Cat, 1000:2000:3 and the reaction were run in solvent free condition at 60° C.	75%	[14]
3		FeP -CMP (5.86 \times 10 ⁻⁷ mol Fe), toluene (3 mL), room temperature (rt), O ₂ (1 atm), Fe/substrate/IBA 1/1000/1000 (molar ratio)	92%	[15]
4	 Ligand	H ₂ O ₂ (1.2 equiv.), Ligand (4.0 mol%), FeCl ₃ ·6H ₂ O (2.0 mol%), THF, rt, 24 h	74%	[16]
5		1000:3000:1 for sulfide/TBAOX/catalyst, rt, air, H ₂ O	90%	[17]
6		TA (0.5 mmol), H₂O₂ (0.25 ml), CH₃CN (10 ml), catalyst (50 mg), temperature (100 °C), and time (13 h)	95%	Our Work

Table S5: Calculated ΔG values of sulfoxide-O and sulfoxide-S pathway for **Fe-Tt-POP** and Fe-Rb-POP, respectively

Free Energy (ΔG) (eV)		
Reaction Pathway	Fe-Tt-POP (planar)	Fe-Rb-POP (non-planar)
Sulfoxide-O	-0.061	-0.097
Sulfoxide-S	-0.017	-0.055

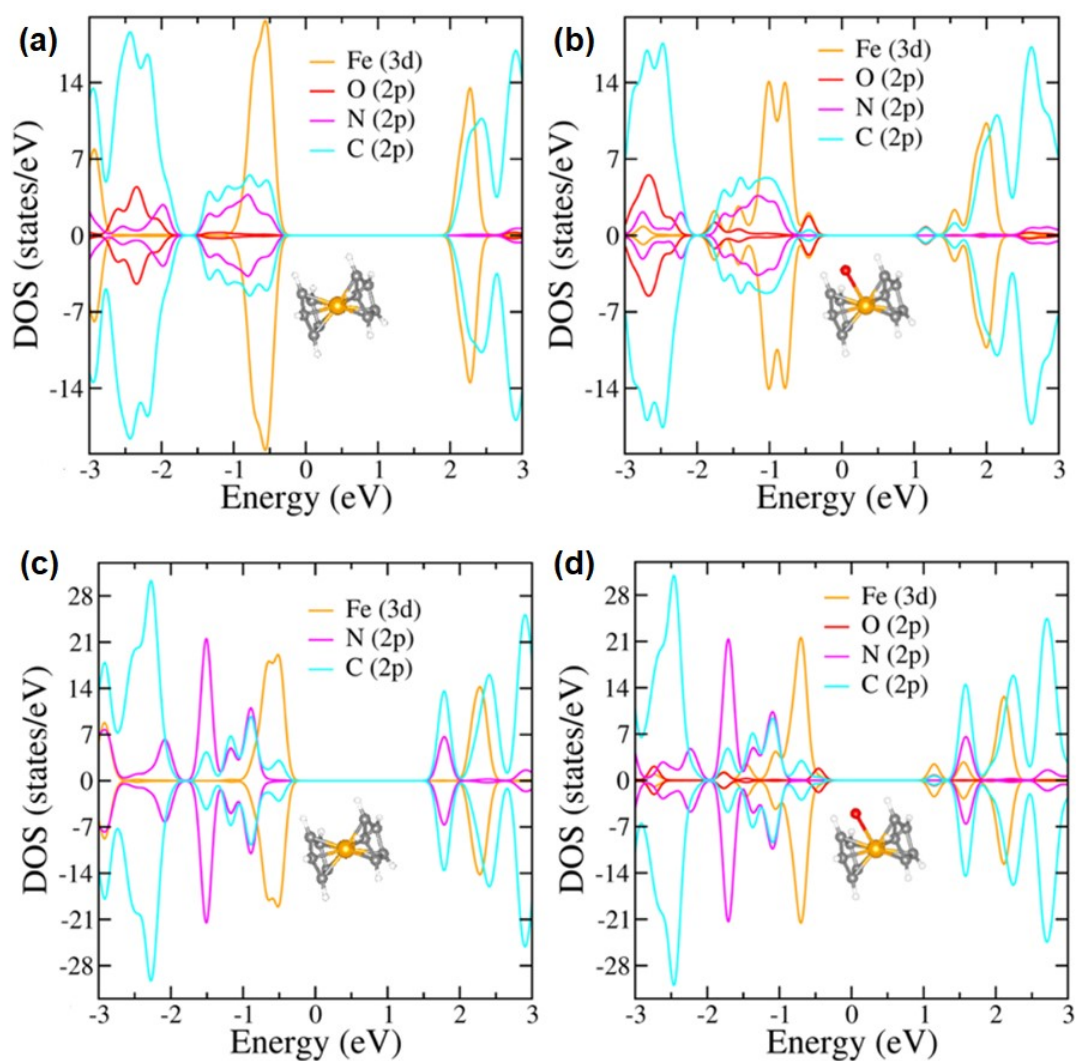


Figure S19: Atom-projected partial density of states (PDOS) of (a) **Fe-Rb-POP** without Fe=O, (b) **Fe-Rb-POP** with Fe=O, (c) **Fe-Tt-POP** without Fe=O, and (d) **Fe-Tt-POP** with Fe=O.

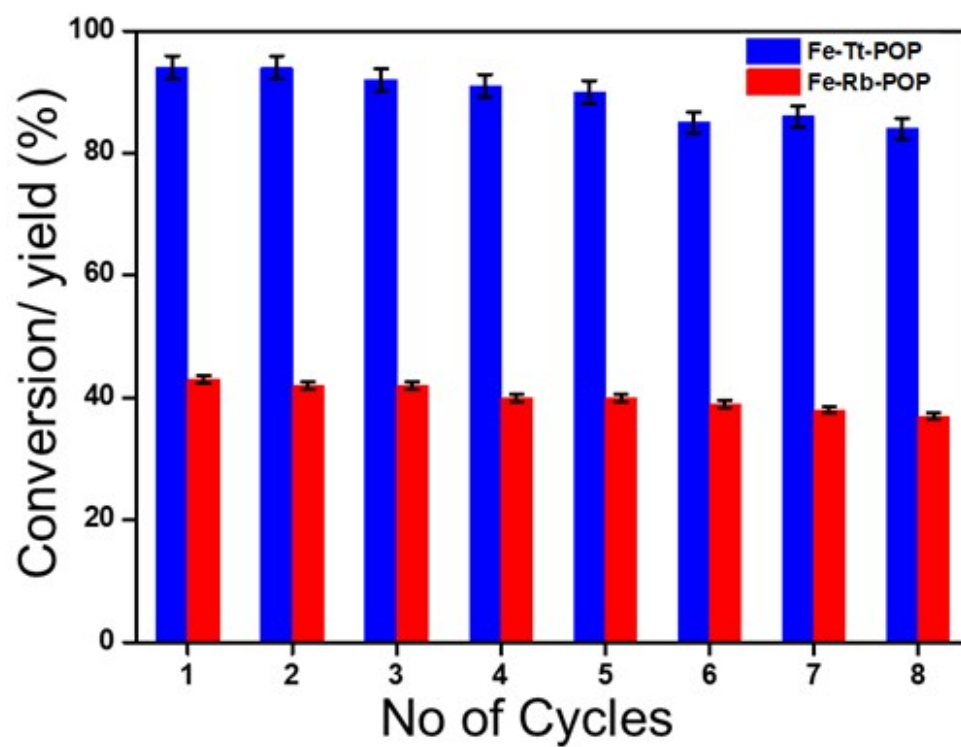


Figure S20: Reusability test of Fe-Tt-POP and Fe-Rb-POP. Reaction conditions: TA (2.5 mmol), H₂O₂ (1.25 ml), CH₃CN (100 ml), catalyst (250 mg), temperature (100 °C), and time (13 h).

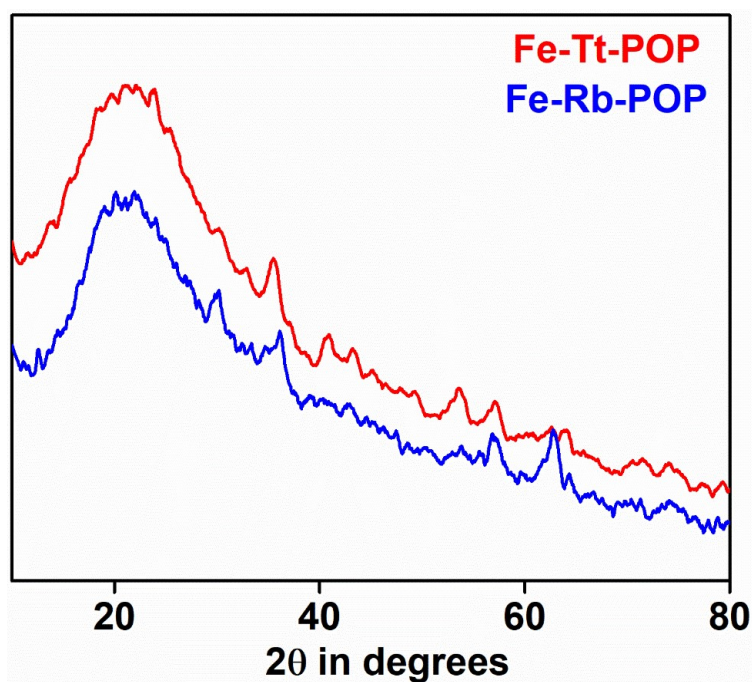


Figure S21: PXRD analysis of reused **Fe-POP** catalysts.

As we have noticed in the PXRD patterns of the used **Fe-POPs**, the overall amorphous nature of the catalyst remains intact, with some occasional low intensity sharp peaks at $2\theta = 35.5^\circ$ and 62.8° . The corresponding low intensity peaks are assigned to very small amount iron oxides formed during the oxidative catalytic conversion of thioanisole.

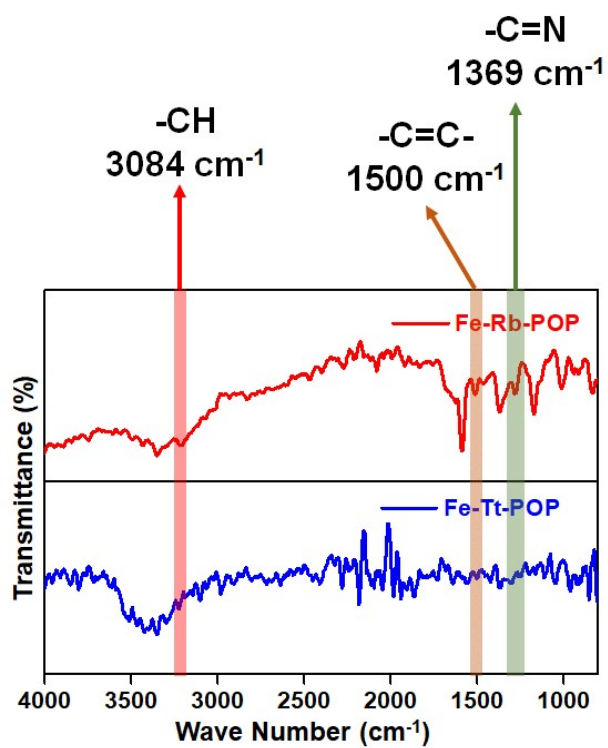


Figure S22: FT-IR analysis of reused catalyst **Fe-Tt-POP** & **Fe-Rb-POP**, respectively.

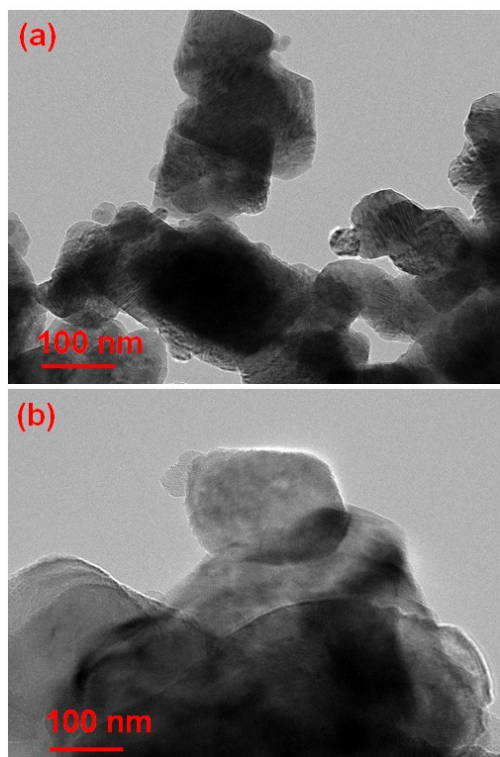


Figure S23: TEM images of reused catalysts **Fe-Tt-POP** (a) and **Fe-Rb-POP** (b), respectively after 8th consecutive catalytic run.

Reusability Test:

As the robustness and reusability are two prime factors to evaluate utility of heterogeneous catalysts in industrial scale, we have performed reusability test for our **Fe-Tt-POP** and **Fe-Rb-POP** catalysts up to 8th catalytic run under optimized reaction condition to unveil the heterogeneity. After each catalytic run, the catalysts are simply filtered off and washed by methanol several times and dried in oven at 80°C, then used for the next cycle. The lack of significant drop in catalytic conversion indicates that the heterogeneity remains unaltered in case of both **Fe-Tt-POP** and **Fe-Rb-POP** catalysts during harsh reaction conditions. This demonstrates that the reactivation process is not necessary to activate the catalyst for further catalytic run. In case of our **Fe-Tt-POP** and **Fe-Rb-POP** catalysts, we have observed negligible decline of TA conversion from 94% to 84% and 43% to 37%, respectively even after 8th catalytic cycle (**Figure S19, SI**). Furthermore, we have also performed PXRD, FT-IR spectroscopy & TEM analysis of the reused **Fe-Tt-POP** and **Fe-Rb-POP** sample to unravel the change in crystallinity and morphology after 8th consecutive catalytic run

compared to fresh catalysts. The PXRD of **Fe-Tt-POP** and **Fe-Rb-POP** demonstrate the amorphous nature of porous organic polymer remain unaltered (**Figure S20, SI**). However, some sharp peaks of lower intensity after 20° appeared in both cases, probably due to the formation of iron oxide species at higher temperature, almost unrecognizable with bare eyes. FT-IR spectra of the reused catalysts (**Figure S21, SI**) clearly illustrate the presence of the secondary amine (N-H) and newly formed methylene (-CH-) linkage on our as-synthesized Fe-POPs even after 8th catalytic run. This indicates structural integrity of the highly robust catalysts remain unaltered. TEM analysis of both catalysts provided in **Figure S22** in SI, clearly demonstrate encapsulated structure of ferrocene aldehyde based porous organic polymer. The darker and gloomy area defined the presence of metal sites and carbonaceous network of M-POP after 8th catalytic run. For both cases, we have observed random organization & overlapping of different geometric patterns, probably due to the exposure of reactive environment up to 8th catalytic run. Although the morphology of **Fe-Tt-POP** and **Fe-Rb-POP** materials are compromised to some extent, but marginal drop-in catalytic activity even after 8th catalytic cycle towards the oxidative decontamination of sulfur mustards indicates the surface reconstruction and reshaping of the M-POP during reaction.

Novelty of our designed Catalytic System & Activity:

The design and development of efficient catalytic systems for the detoxification chemical warfare agents (CWAs) such as sulfur mustard are immensely relevant to protect the world from manmade disasters. The blistering agent mustard gas generally utilized as a chemical weapon during war and people suffered from blisters upon contact with skin, eyes, lungs or any other mucous membrane and long-term consequence of it. Mustard gas actually acts as alkylating agent, which prevent the protein synthesis in the human body by inhibiting transcription of DNA and RNA. Recently, inter-governmental Organisation for the Prohibition of Chemical Weapons (OPCW) declared that 97% stock piles of chemical weapons should destroyed at Chemical Weapons Convention, attended by 193 countries. The total amount of such stockpiles of warfare agents recorded 70,000 metric tons and a huge amount of portion is left behind due lack of authentic detoxification pathway, remain a great challenge to the scientific community. There are three possible pathways to detoxify sulfur mustard, hydrolysis, dehydrohalogenation and halogenation. But, the first two processes led to the formation toxic HCl by-product, are less suitable for the detoxification. The most promising approach is selective oxidation of sulfur mustard, which leads to the formation of benign sulfoxide (SO). But the over oxidation afforded sulfone (SO₂), which exhibited similar toxicity like mustard gas.^{18,19}

Bleach powders with the varying formulations were the first used as oxidative decontaminants for the HD, but they suffered from various drawbacks including (i) significant diminishment of the activity with time; (ii) huge quantity of bleach is employed for decontamination & (iii) its corrosive nature.²⁰ Although, Metal Oxides, Polyoxometalates and MOFs widely utilized for the detoxification the problem remain unsolved for real time utilization due to various issues including stability, reusability and leaching of active site.²¹ Hence, the development of stable heterogeneous catalyst for selective oxidation of mustard gas remains a challenge to the researchers. In order the bridging the gap between activity and stability in MOFs, we have developed an effective strategy to incorporate metal active sites on porous organic polymer (POP) by considering exceptional advantages of POP framework including high mechanical and chemical stabilities, adjustable chemical functionality and high specific surface area and well-defined pores. The balanced characteristic feature consisting covalent bonds (structural stability) & open metal sites (single-site catalysis) in case of our Fe-POPs appeared as efficient catalyst for selective oxidation of mustard gas. Moreover, introduction of non-planar and planar catalytic core inside **Fe-Rb-POP**, **Fe-Tt-POP** efficiently modulate the catalytic activity by lowering the stretching frequency of Fe-O

bond from ~ 1772 to ~ 1750 cm^{-1} during selective oxidation process as well as decrease Gibbs free energy (ΔG), confirmed from *In-situ* DRIFTS and DFT computational study. As a result, Fe-Tt-POP exhibited almost 99% conversion with more than 78% sulfoxide selectivity of different sulfur mustard derivatives such as 2-Chloroethyl ethyl sulfide (CEES), 2-Chloroethyl methyl sulfide (CEMS), dimethyl sulfide (DMS) etc and the recyclability test also confirmed the stability of the catalyst up to 8th catalytic run. So, the quest of discovering of the ideal catalytic system for the detoxification of mustard gas has been satisfied, which is extremely significant to prevent numerous health problems related to the exposure of sulfur mustard.

References:

- [1] M. J. Frisch, G. W. Trucks, H. B. Schlegel, G. E. Scuseria, M. A. Robb, J. R. Cheeseman, G. Scalmani, V. Barone, G. A. Peterson, H. Nakatsuji, X. Li, M. Caricato, A. V. Marenich, J. Bloino, B. G. Janesko, R. Gomperts, B. Mennucci, H. P. Hratchian, J. V. Ortiz, A. F. Izmaylov, J. L. Sonnenberg, D. Williams-Young, F. Ding, F. Lipparini, F. Egidi, J. Goings, B. Peng, A. Petrone, T. Henderson, D. Ranasinghe, V. G. Zakrzewski, J. Gao, N. Rega, G. Zheng, W. Liang, M. Hada, M. Ehara, K. Toyota, R. Fukuda, J. Hasegawa, M. Ishida, T. Nakajima, Y. Honda, O. Kitao, H. Nakai, T. Vreven, K. Throssell, J. A. Montgomery Jr, J. E. Peralta, F. Ogliaro, M. J. Bearpark, J. J. Heyd, E. N. Brothers, K. N. Kudin, V. N. Staroverov, T. A. Keith, R. Kobayashi, J. Normand, K. Raghavachari, A. P. Rendell, J. C. Burant, S. S. Iyengar, J. Tomasi, M. Cossi, J. M. Millam, M. Klene, C. Adamo, R. Cammi, J. W. Ochterski, R. L. Martin, K. Morokuma, O. Farkas, J. B. Foresman, D. J. Fox, *Gaussian 16 Rev.A*. **2016**, 03.
- [2] A. D. Becke, *J. Chem. Phys.* **1993**, 98, 5648.
- [3] A. Schäfer, H. Horn, R. Ahlrichs, *J. Chem. Phys.* **1992**, 97, 2571-2577.
- [4] K. Eichkorn, F. Weigend, O. Treutler, R. Ahlrichs, *Theor. Chem. Acc.* **1997**, 97, 119-124.
- [5] J. -G. Flores, S. E. P. Figueroa, R. M. D. Castillo, A. Martinez, L. E. Sansores, E. Ramos, *Struct. Chem.* **2021**, 32, 775-785.
- [6] G. Kresse, J. Furthmuller, *Comput. Mater. Sci.* **1996**, 6, 15-50.
- [7] P. E. Blochl, *Phys. Rev. B*, **1994**, 50, 17953-17979.
- [8] J. P. Perdew, K. Burke, M. Ernzerhof, *Phys. Rev. Lett.* **1996**, 77, 3865-3868.
- [9] G. Marzano, D. Kotowski, F. Babudri, R. Musio, A. Pellegrino, S. Luzzati, R. Po, G. M. Farinola, *Macromolecules* **2015**, 48, 7039-7048.
- [10] Q. Wang, Y. Wang, W. Zheng, B. Shahid, M. Qiu, D. Wang, D. Zhu, R. Yang, *ACS Appl. Mater. Interfaces* **2017**, 9(37), 32126-32134.
- [11] X. Sheng, H. Gao, Y. Zhou, B. Wang, X. Sha, *Appl. Organomet. Chem.* **2019**, 33, e4979.
- [12] B. Zhou, L. Liu, Z. Yang, X. Li, Z. Wen, L. Chen, *ChemElectroChem* **2019**, 6, 485-492.
- [13] Y. Ferrand, R. Daviaud, P. L. Maux, G. Simonneaux, *Tetrahedron: Asymmetry* **2006**, 17, 952-960.
- [14] M. Jafarpour, A. Rezaeifard, F. Feizpour, *Chemistry Select* **2017**, 2, 2901-2909.

- [15] L. Chen, Y. Yang, D. Jiang, *J. Am. Chem. Soc.* **2010**, *132*, 9138-9143.
- [16] K. A. Stingl, K. M. Weiß, S. B. Tsogoeva, *Tetrahedron* **2012**, *68*, 8493-8501.
- [17] A. Rezaeifard, M. Jafarpour, *Catal. Sci. Technol.* **2014**, *4*, 1960-1969.
- [18] J. Hirade, A. Ninomiya, *J. Biochem.* **1950**, *37*, 19-34.
- [19] R. W. Baker, *Ind. Eng. Chem. Res.* **2002**, *41*, 1925-1928.
- [20] M.C. DeRosa, R.J. Crutchley, *Coord. Chem. Rev.* **2002**, *233-234*, 351-371.
- [21] C. T. Buru, P. Li, B. L. Mehdi, A. Dohnalkova, A. E. PlateroPrats, N. D. Browning, K. W. Chapman, J. T. Hupp and O. K. Farha, *Chem. Mater.* **2017**, *29*, 5174-5181.